Hybrid Arrays: How Many RF Chains Are Required to Prevent Beam Squint?

Heedong Do, *Member, IEEE*, Namyoon Lee, *Senior Member, IEEE*, Robert W. Heath Jr., *Fellow, IEEE*, Angel Lozano, *Fellow, IEEE*

Abstract—With increasing frequencies, bandwidths, and array apertures, the phenomenon of beam squint arises as a serious impairment to beamforming. Fully digital arrays with true time delay per antenna element are a potential solution, but they require downconversion at each element. This paper shows that hybrid arrays can perform essentially as well as digital arrays once the number of radio-frequency chains exceeds a certain threshold that is far below the number of elements. This threshold is determined by only a few physical parameters—bandwidth, array size, and beamforming direction—and can be expressed in a remarkably simple closed form. The result is robust, holding also for suboptimum yet highly appealing beamspace architectures.

Index Terms—Wideband communication, beam squint, hybrid beamforming, mmWave frequencies, terahertz frequencies

I. Introduction

In the quest for fresh spectrum, there is much interest in millimeter wave (mmWave) and sub-terahertz bands [1]. Enormous amounts of bandwidth can be put into service at these frequencies, contingent on high-gain antennas to overcome the rising noise floor [2]-[5]. For the sake of reconfigurability, antenna arrays composed of multiple lowgain elements are preferred over a single high-gain antenna. Given that hundreds of such elements become necessary, fully digital arrays with one radio-frequency (RF) chain per element are unaffordable in terms of power consumption and cost [6]-[8]. Fully analog designs with one RF chain per array must instead be embraced. The drawback is then that, while the channel is frequency-dependent, analog phase shifters are frequency-independent. This results in diminished antenna gains at frequencies away from the central one, at which the array is optimized, in a phenomenon termed beam squint [9, Ch. 1.2].

While this phenomenon can in principle be corrected with true-time-delay (TTD) beamforming [10]–[14], the required

H. Do and N. Lee are with the School of Electrical Engineering, Korea University, 02841 Seoul, South Korea (e-mail: {doheedong, namyoon}@korea.ac.kr). Their work is supported in part by the Institute of Information & Communications Technology Planning & Evaluation (IITP) under Grant 2021-0-00161 and in part by the National Research Foundation of Korea (NRF) under Grant 2023-00208552, both funded by the Korea Government (MSIT). Robert W. Heath Jr. is with the Department of Electrical and Computer Engineering, University of California at San Diego, La Jolla, CA 92093 USA (e-mail: rwheathjr@ucsd.edu). His work is supported in part by the National Science Foundation under grant nos. NSF-ECCS-2153698, NSF-CCF-2225555, NSF-CNS-2147955, and in part by funds from federal agency and industry partners as specified in the Resilient & Intelligent NextG Systems (RINGS) program. A. Lozano is with Univ. Pompeu Fabra, 08018 Barcelona (e-mail: angel.lozano@upf.edu). His work is supported by the Maria de Maeztu Units of Excellence Programme (MDM-2021-001195-M), by the Fractus-UPF Chair on Tech Transfer and 6G, and by ICREA.

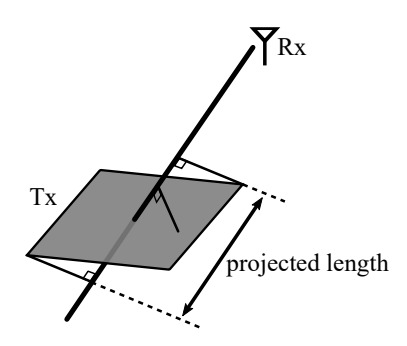


Fig. 1. Projection of a planar array onto the direction of beamforming, yielding a line segment.

delays for array sizes of interest are not available at mmWave frequencies when implemented at RF (see [15, Table I] and [16, Table I]) and, in any event, a large chip area would be consumed. Digital true-time-delay beamforming does offer a much broader range of delays [16, Table II], but again it necessitates of downconversion to baseband at each antenna element. Hybrid arrays lie between the two extremes, fully analog and fully digital, as they feature a number of RF chains that is above one but below the number of antenna elements. Potentially then, hybrid arrays can bridge these extremes in terms of performance and cost, and their beam-squint analysis is therefore of importance. However, in contrast with fully analog arrays, for which the beam-squint loss has been quantified with theoretical guarantees [9], only algorithmic approaches are available for hybrid arrays [17]–[21]. Relevant contributions in the literature include [22]–[26], which address different aspects: codebook design for analog arrays [22], [23], channel estimation [24], and beamforming optimization problem with an additional use of true time delay [25], [26].

In the wake of these recent contributions, this paper tackles the following research questions:

- 1) What is the loss in beamforming gain caused by squint when using hybrid arrays instead of fully digital ones?
- 2) Is there a number of RF chains beyond which this loss vanishes and, if so, what is that number?

Remarkably, the latter question is answered in the affirmative. The minimum number of RF chains required to eradicate the beam-squint loss emerges in a compact closed form. For a linear array, this minimum number is shown to be simply

$$\frac{\text{bandwidth}}{\text{carrier frequency}} \cdot \frac{\text{projected length}}{\text{wavelength}} \tag{1}$$

where "projected length" refers to the array's projection onto the direction of beamforming. The above extends readily to

TABLE I NOTATION

Notation	Description
$span(v_1,\ldots,v_n)$	Span of vectors v_1, \ldots, v_n
$\dim V$	Dimension of a vector space V
$\ a\ $	Euclidean norm of a vector \boldsymbol{a}
$oldsymbol{A}^{ op}$	Transpose of a matrix \boldsymbol{A}
$oldsymbol{A}^*$	Conjugate transpose of a matrix A
$oldsymbol{A}^{1/2}$	Positive square root of a semi-definite matrix A
$\mathrm{tr}oldsymbol{A}$	Trace of a matrix \boldsymbol{A}
$\boldsymbol{A}_1 \otimes \boldsymbol{A}_2$	Kronecker product of matrices A_1 and A_2
$blkdiag(\boldsymbol{A}_1,\ldots,\boldsymbol{A}_n)$	Block diagonal matrix with blocks A_1, \ldots, A_n
$\lambda_\ell(\cdot)$	ℓ th largest eigenvalue of a matrix or operator
$L^2(\cdot)$	Space of square integrable functions
[•]	Iverson bracket
•	Set cardinality
[·]	Ceiling function
$\operatorname{sinc}(x) \equiv \frac{\sin \pi x}{\pi x}$ $f(x) = o(g(x))$	Sinc function
f(x) = o(g(x))	$f(x)/g(x) \to 0$ as $x \to \infty$
$f(x) = \mathcal{O}(g(x))$	There exist constants C and x_0 such that
	$ f(x) \le Cg(x)$ for all $x \ge x_0$

planar arrays, only with that projected length generalized to being the length of the longest segment that the array projects onto the direction of beamforming (see Fig. 1).

As the product of carrier frequency and wavelength equals the speed of light, (1) can equivalently be expressed as

$$\frac{1}{c}$$
 · bandwidth · projected length. (2)

In rather broad generality, this product of the bandwidth and the projected array length dictates the severity of the beam squint, and it directly gives the minimum number of RF chains required for squint-free beamforming with a hybrid array. Growing bandwidths, expanding array apertures, and beamforming directions deviating from broadside, all aggravate the squint and increase the value of (2), yet a hybrid array equipped with that number of chains can always beamform without squint. (This behavior is asymptotic, in the sense that the squint vanishes as the product grows large, yet it very faithfully describes the behavior for values of interest.)

For an array intending to beamform in any direction, the projected length in (2) must be set to its worst—highestvalue, which is the actual length (for a linear array) or the diagonal length (for a planar array).

The findings summarized above are robust, holding not only for optimum beamforming, but further for suboptimal beamspace architectures consisting of a bank of beams with a regular disposition [27].

The existence of a number of RF chains beyond which the squint vanishes is proved to hold even if the connectivity within the hybrid array is restricted, in the so-called hybridlyconnected structure where the array is partitioned into subarrays and each subarray is connected only to a subset of RF chains. An interesting tradeoff then arises between the number of analog phase shifters and the number of RF chains, with some residual beam squint becoming inevitable if both are simultaneously reduced.

The paper is organized as follows. Sec. II introduces the system model and Sec. III describes the phenomenon of beam squint. A simple criterion for squint-free operation is set

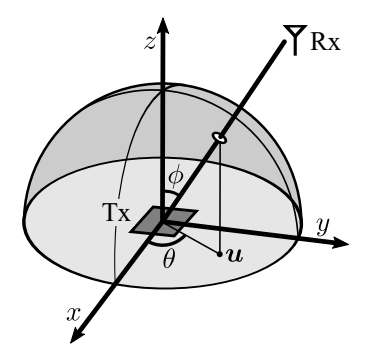


Fig. 2. Considered geometry, including u and a unit hemisphere as reference.

forth in Sec. IV. Then, the minimum number of RF chains required for squint-free operation is quantified for linear and planar arrays in Secs. V and VI, respectively. The foregoing analyses are numerically validated in Sec. VII. In Sec. VIII, the results are extended to simpler architectures with restricted connectivity, and also to a multiantenna receiver. Finally, the paper concludes in Sec. IX.

For a summary of the notation employed throughout the manuscript, readers are referred to Table I.

II. SYSTEM MODEL

A. Array Model

Consider a transmitter equipping a uniform planar array (UPA) communicating with a single-antenna receiver. The UPA has dimensionality $N_x imes N_y$ and aperture $L_x imes L_y,$ whereby the element spacings along the respective dimensions are $d_x = \frac{L_x}{N_x}$ and $d_y = \frac{L_y}{N_y}$.

The coordinate system is such that the nth transmit element

 $(n \in \{0,\ldots,N-1\} \text{ with } N=N_xN_y) \text{ is at }$

$$\begin{bmatrix} x_n & y_n & 0 \end{bmatrix}^\top = \begin{bmatrix} d_x \left(n_x - \frac{N_x - 1}{2} \right) & d_y \left(n_y - \frac{N_y - 1}{2} \right) & 0 \end{bmatrix}^\top$$

where $n_x \in \{0, \dots, N_x - 1\}$ and $n_y \in \{0, \dots, N_y - 1\}$ are the quotient and remainder of n/N_y , respectively. The receiver is located at $D \left[\sin \phi \cos \theta \quad \sin \phi \sin \theta \quad \cos \phi \right]^{\top}$ where D is the communication range, ϕ is the zenith angle, and θ is the azimuth angle (see Fig. 2). For convenience, let us henceforth define

$$\boldsymbol{r}_n = \begin{bmatrix} x_n & y_n \end{bmatrix}^{\top} \qquad \boldsymbol{u} = \begin{bmatrix} u_x & u_y \end{bmatrix}^{\top}$$
 (3)

where $u_x = \sin \phi \cos \theta$ and $u_y = \sin \phi \sin \theta$. Note that u, also depicted in Fig. 2, corresponds to the uv-coordinates, handy for many applications including array signal processing [28]. It is a convenient two-dimensional projection of the unitvector pointing to the receiver; the higher its magnitude, the further from broadside, with $\|u\| = 0$ and $\|u\| = 1$ respectively denoting the exact broadside and endfire directions.

The consideration of UPAs does not exclude uniform linear arrays (ULAs), as the latter are a special case of the former. Our convention for linear arrays is to set $N_y = 1$.

B. Channel Model

We posit a line-of-sight (LOS) connection in the far field. Denoting the carrier frequency by f_c , and the frequency relative to it by $f \in [-\frac{W}{2}, \frac{W}{2}]$ with W the bandwidth, the nth entry of the normalized channel vector \boldsymbol{a}^* at $f_c + f$ is

$$[\boldsymbol{a}^*(f)]_n = \exp\left(j2\pi \frac{f_c + f}{c} \boldsymbol{u}^\top \boldsymbol{r}_n\right). \tag{4}$$

Such channel vector can be expressed as [9, Eq. 1.59]

$$\boldsymbol{a}^*(f) = \boldsymbol{a}_x^*(f) \otimes \boldsymbol{a}_y^*(f) \tag{5}$$

where $a_x(f) \in \mathbb{C}^{N_x}$ and $a_y(f) \in \mathbb{C}^{N_y}$ are vectors with entries

$$[\boldsymbol{a}_x^*(f)]_n = \exp\left(j2\pi \frac{f_c + f}{c} u_x x_n\right) \tag{6}$$

$$[\boldsymbol{a}_{y}^{*}(f)]_{n} = \exp\left(j2\pi \frac{f_{c} + f}{c} u_{y} y_{n}\right). \tag{7}$$

The amplitude factor omitted by the normalization can be directly incorporated into the signal-to-noise ratio, giving¹

$$SNR = \frac{\lambda^2 G_t G_r P_t}{(4\pi D)^2 W N_0} \tag{8}$$

where $G_{\rm t}$ and $G_{\rm r}$ are the transmit and receive element gains, $P_{\rm t}$ is the total radiated power, and N_0 is the noise spectral density.

C. Signal Model

A hybrid array is considered, with the number of RF chains being $N_{\rm RF}$. Denoting the analog and digital beamforming stages by $\mathbf{W}_{\rm a} \in \mathbb{C}^{N \times N_{\rm RF}}$ and $\mathbf{w}_{\rm d}(f) \in \mathbb{C}^{N_{\rm RF}}$, respectively, the relation between the transmit signal s(f) and the receive signal y(f) is given by

$$y(f) = \boldsymbol{a}^*(f)\boldsymbol{W}_{\mathsf{a}}\boldsymbol{w}_{\mathsf{d}}(f)s(f) + v(f) \tag{9}$$

where v(f) is a white Gaussian noise process with unit power spectral density. A single signal stream is transmitted, as the channel is of rank one.

Letting s(f) have unit power, the power constraint becomes

$$\frac{1}{W} \int_{-\frac{W}{2}}^{\frac{W}{2}} \| \boldsymbol{W}_{\mathsf{a}} \boldsymbol{w}_{\mathsf{d}}(f) \|^{2} df = \mathsf{SNR}. \tag{10}$$

Introducing

$$p(f) = \|\mathbf{W}_{\mathsf{a}}\mathbf{w}_{\mathsf{d}}(f)\|^2 \tag{11}$$

$$g(f) = \frac{|a^*(f)W_{a}w_{d}(f)|^2}{\|W_{a}w_{d}(f)\|^2},$$
(12)

we can succinctly rewrite the signal model as

$$y(f) = \sqrt{g(f)p(f)}s(f) + v(f) \tag{13}$$

with the streamlined power constraint

$$\frac{1}{W} \int_{-\frac{W}{2}}^{\frac{W}{2}} p(f) df = \mathsf{SNR}. \tag{14}$$

Respectively, g(f) and p(f) can be interpreted as the beamforming gain and transmit power at frequency f.

For a given analog beamformer, we can optimize the digital beamformer. To do so, we introduce the auxiliary quantity [30, Lemma 5]

$$\tilde{\mathbf{w}}_{\mathsf{d}}(f) \equiv (\mathbf{W}_{\mathsf{a}}^* \mathbf{W}_{\mathsf{a}})^{\frac{1}{2}} \mathbf{w}_{\mathsf{d}}(f), \tag{15}$$

which is a natural choice from

$$p(f) = \mathbf{w}_{\mathsf{d}}^{*}(f)(\mathbf{W}_{\mathsf{a}}^{*}\mathbf{W}_{\mathsf{a}})\mathbf{w}_{\mathsf{d}}(f)$$
 (16)

$$= \|\tilde{\boldsymbol{w}}_{\mathsf{d}}(f)\|^2. \tag{17}$$

Plugging (15) into (12), we obtain

$$g(f) = \frac{\|\boldsymbol{a}^*(f)\boldsymbol{W}_{\mathsf{a}}(\boldsymbol{W}_{\mathsf{a}}^*\boldsymbol{W}_{\mathsf{a}})^{-\frac{1}{2}}\tilde{\boldsymbol{w}}_{\mathsf{d}}(f)\|^2}{\|\tilde{\boldsymbol{w}}_{\mathsf{d}}(f)\|^2}$$
(18)

$$\leq \|(\boldsymbol{W}_{\mathsf{a}}^* \boldsymbol{W}_{\mathsf{a}})^{-\frac{1}{2}} \boldsymbol{W}_{\mathsf{a}}^* \boldsymbol{a}(f)\|^2$$
 (19)

where the upper bound follows from the Cauchy-Schwarz inequality. For any p(f), such bound can be attained by

$$\tilde{w}_{d}(f) = \sqrt{p(f)} \frac{(W_{a}^{*}W_{a})^{-\frac{1}{2}} W_{a}^{*}a(f)}{\|(W_{a}^{*}W_{a})^{-\frac{1}{2}} W_{a}^{*}a(f)\|}.$$
 (20)

III. BEAM SQUINT

The beam squint can be evidenced by observing how the beamforming gain behaves on the space-frequency plane. To make the dependence on both space and frequency explicit, in this section the notations a(u, f) and g(u, f) are used in lieu of a(f) and g(f) when appropriate.

With a unit-norm analog combiner w_a and no digital combiner, (12) reduces to

$$g(\boldsymbol{u}, f) = |\boldsymbol{w}_{\mathsf{a}}^* \boldsymbol{a}(\boldsymbol{u}, f)|^2, \tag{21}$$

which is often termed *beam pattern* in terms of its dependence on u [9]. From (4),

$$a^*(u, f) = a^*((1 + f/f_c)u, 0),$$
 (22)

which gives

$$g(\boldsymbol{u}, f) = g((1 + f/f_c)\boldsymbol{u}, 0). \tag{23}$$

The beam pattern is hence frequency-dependent, and the peak of the beam changes its direction with frequency, which is why the phenomenon is termed squint; only perfectly broadside beams (u=0) are immune. This argument is valid for any array geometry and beamformer, thus it is essentially a generalization of [26, Lemma 2].

As a guideline for when the squint becomes significant, the notion of 3-dB loss in beamforming gain is often used [9, Ch. 1.2]. For ease of exposition, consider an N-element ULA on the x-axis and maximum ratio transmission (MRT), whereby $w_a = \frac{a(0)}{\sqrt{N}}$. Then,

$$g(f) = \frac{|\mathbf{a}^*(f)\mathbf{a}(0)|^2}{N}$$
 (24)

$$= \frac{1}{N} \left| \sum_{n=0}^{N-1} e^{-j2\pi \frac{f d_x u_x}{c} n} \right|^2$$
 (25)

$$=F_N\left(\frac{2\pi d_x u_x}{c}f\right) \tag{26}$$

¹Large-scale effects such as atmospheric attenuation [29], which is not negligible for long-range transmissions, can be easily incorporated.

with $F_N(x) = \frac{1}{N} \left(\frac{\sin \frac{Nx}{2}}{\sin \frac{x}{2}} \right)^2$. The 3-dB loss occurs when

$$F_N\left(\frac{\pi d_x u_x}{c}W\right) = \frac{N}{2}. (27)$$

Given the array length $L_x = Nd_x$, the argument of $F_N(\cdot)$ above suggests defining

$$\alpha \equiv \frac{W}{f_c} \frac{L_x u_x}{\lambda} \tag{28}$$

and, indeed, this product of the normalized bandwidth and normalized projected aperture—termed *channel dispersion* factor in [27]—turns out to be an excellent measure of the squint intensity with analog beamforming and plays a central role in the remainder of the paper. With it, (27) becomes

$$F_N\left(\frac{\pi\alpha}{N}\right) = \frac{N}{2} \tag{29}$$

and, as $N \to \infty$, this boils down to

$$\operatorname{sinc}^2 \frac{\alpha}{2} = \frac{1}{2},\tag{30}$$

whose numerical solution gives

$$\alpha_{3dB} \approx 0.886.$$
 (31)

As shown in App. A, α_{3dB} decreases with N and the convergence to 0.886 is quick, hence this value holds virtually for any N; the error is only 5% for N = 3 [31, Fig. 2.4].

Just like a 3-dB loss in beamforming gain maps to α_{3dB} , any other loss value has its corresponding α .

To keep α constant, so as to maintain the beam squint at a given level, (28) dictates that:

- the larger the bandwidth, the smaller the array must be;
- the further the beam points from the broadside direction, the smaller the bandwidth and/or the array must be.

It is henceforth assumed that $\alpha \neq 0$, for otherwise there is no beam squint in the first place.

IV. APPROACHING SQUINT-FREE PERFORMANCE

In this section, a simple criterion is introduced to determine whether the beamformer is approaching squint-free performance.

A. Average Beamforming Gain

Let us define the average beamforming gain

$$g_{\text{avg}} = \frac{1}{W} \int_{-\frac{W}{2}}^{\frac{W}{2}} g(f) df$$
 (32)

and, by means of the positive definite matrix

$$\boldsymbol{B} = \frac{1}{W} \int_{-\frac{W}{2}}^{\frac{W}{2}} \boldsymbol{a}(f) \boldsymbol{a}^*(f) df, \tag{33}$$

further express such average gain as [32, Eq. 20]

$$g_{\mathsf{avg}} = \frac{1}{W} \int_{-\frac{W}{2}}^{\frac{W}{2}} \|\boldsymbol{a}^*(f) \boldsymbol{W}_{\mathsf{a}}(\boldsymbol{W}_{\mathsf{a}}^* \boldsymbol{W}_{\mathsf{a}})^{-\frac{1}{2}} \|^2 df$$
 (34)

$$= \operatorname{tr}(\boldsymbol{W}_{\mathsf{a}}(\boldsymbol{W}_{\mathsf{a}}^* \boldsymbol{W}_{\mathsf{a}})^{-1} \boldsymbol{W}_{\mathsf{a}}^* \boldsymbol{B}). \tag{35}$$

Note that

$$[\boldsymbol{B}]_{n',n} = \frac{1}{W} \int_{-\frac{W}{2}}^{\frac{W}{2}} \exp\left(j2\pi \frac{f_{c} + f}{c} \boldsymbol{u}^{\top} (\boldsymbol{r}_{n} - \boldsymbol{r}_{n'})\right) df$$
(36)

and, as far as the eigenvalues of B are concerned, the term

$$\exp\left(j2\pi\frac{f_{\rm c}}{c}\boldsymbol{u}^{\top}(\boldsymbol{r}_n-\boldsymbol{r}_{n'})\right) \tag{37}$$

is irrelevant. This is because (37) has the same effect as two unitary diagonal matrices, and the eigenvalues are similarity invariant [33, Thm. 1.3.3]. Therefore, without loss of generality in terms of the eigenvalues, we can let $f_c = 0$ to obtain

$$[\boldsymbol{B}]_{n',n} = \frac{1}{W} \int_{-\frac{W}{2}}^{\frac{W}{2}} \exp\left(j2\pi \frac{f}{c} \boldsymbol{u}^{\top} (\boldsymbol{r}_n - \boldsymbol{r}_{n'})\right) df$$
 (38)

$$= \operatorname{sinc}\left(\frac{W \boldsymbol{u}^{\top} (\boldsymbol{r}_n - \boldsymbol{r}_{n'})}{c}\right). \tag{39}$$

B. Simple Criterion for Squint-Free Performance

With fully digital beamforming, the squint can be eradicated to attain g(f) = N. Since $g(f) \leq N$, it follows that $g_{\text{avg}} = N$ is a necessary and sufficient condition for g(f) = N. Thus, $g_{\text{avg}} \approx N$ is a simple criterion to determine whether the beamformer is approaching squint-free performance.

C. Analog Beamformer Maximizing the Average Beamforming Gain

Given $\lambda_{\ell}(B)$ as the ℓ th largest eigenvalue of B, and u_{ℓ} as the corresponding unit-norm eigenvector, g_{avg} is maximized by [32, Prop. 1]

$$\boldsymbol{W}_{\mathsf{a}} = \begin{bmatrix} \boldsymbol{u}_0 & \cdots & \boldsymbol{u}_{N_{\mathsf{PF}}-1} \end{bmatrix} \tag{40}$$

at

$$g_{\text{avg}} = \sum_{\ell < N_{\text{e-r}}} \lambda_{\ell}(\boldsymbol{B}). \tag{41}$$

Note that

$$\sum_{\ell} \lambda_{\ell}(\mathbf{B}) = \operatorname{tr}(\mathbf{B}) = N \tag{42}$$

consistent with the fact that an all-digital implementation $(N_{\mathsf{RF}}=N)$ incurs no beam squint.

V. LINEAR ARRAYS

Before embarking on the analysis with UPAs, let us first entertain the simpler ULA case, with $N_y=1$. Then, in Sec. VI, the UPA results will be built upon the results presented herein.

A. Continuous-Aperture Representation

From (41), the eigenvalues of \boldsymbol{B} are of great importance. For the sake of analysis, we move into the continuous realm by replacing the discrete array with a continuous one.

For linear arrays, (39) reduces to

$$[\boldsymbol{B}]_{n',n} = \operatorname{sinc}\left(\frac{Wu_x d_x (n-n')}{c}\right) \tag{43}$$

$$= \operatorname{sinc} \frac{\alpha(n'-n)}{N}. \tag{44}$$

where, recall from Sec. III, α measures the squint intensity that would be experienced with purely analog beamforming. The even nature of (44) with respect to α enables assuming $\alpha > 0$ without loss of generality. The continuous counterpart to \boldsymbol{B} is the integral operator [34, Sec. V]

$$\mathcal{B}_{\alpha}: L^{2}(\mathbb{R}) \to L^{2}(\mathbb{R})$$

$$s(r) \mapsto \int B_{\alpha}(r', r) s(r) dr$$

$$(45)$$

where

$$B_{\alpha}(r',r) = \alpha \operatorname{sinc}(\alpha(r-r'))[r \in I][r' \in I]$$
 (46)

is the kernel with $I = [-\frac{1}{2}, \frac{1}{2}]$. Here, $[\cdot]$ denotes the Iverson bracket [35]

$$[condition] \equiv \begin{cases} 1 & \text{the condition is true} \\ 0 & \text{otherwise} \end{cases}$$
 (47)

The matrix B can be recovered from (46) by sampling at the normalized antenna element coordinates, namely

$$[\boldsymbol{B}]_{n',n} = \frac{1}{\alpha} B_{\alpha} \left(\frac{r_{n'}}{L_x}, \frac{r_n}{L_x} \right), \tag{48}$$

where the normalization by $\frac{1}{\alpha}$ is convenient, as evidenced in subsequent sections. In terms of eigenvalues, the continuous representation becomes exact as the element spacings vanish, namely [34, Sec. V-C]

$$\frac{\alpha}{N}\lambda_{\ell}(\mathbf{B}) \to \lambda_{\ell}(\mathcal{B}_{\alpha}) \tag{49}$$

in Euclidean norm.

The squint-free condition with hybrid beamforming, $\sum_{\ell < N_{\rm RF}} \lambda_\ell({\bm B}) \approx N,$ translates to

$$\sum_{\ell \le N_{\rm DF}} \lambda_{\ell}(\mathcal{B}_{\alpha}) \approx \alpha \tag{50}$$

and the counterpart to the all-digital extreme in (42) is $\sum_{\ell} \lambda_{\ell}(\mathcal{B}_{\alpha}) = \alpha$.

The continuous-aperture representation introduced herein is an analytically friendly proxy to the discrete model, and its practical relevance is confirmed by thorough numerical studies.

B. Eigenvalue Behavior

The eigenvalues of \mathcal{B}_{α} are well studied [36] (see [37] for its relevance to bandlimited signals). In particular, they are bounded above by 1 and asymptotically polarized into two levels. Precisely, as $\alpha \to \infty$,

$$|\{\ell : \lambda_{\ell}(\mathcal{B}_{\alpha}) > \epsilon\}| = \alpha + \mathcal{O}(\log \alpha) \tag{51}$$

for any $\epsilon \in (0,1)$. Put another way,

$$[\lambda_0(\mathcal{B}_{\alpha}), \lambda_1(\mathcal{B}_{\alpha}), \ldots] \approx [\underbrace{1, \ldots, 1}_{\approx \alpha}, 0, \ldots]$$
 (52)

where the approximations sharpen as α grows.

C. Number of Required RF chains

Let us consider the asymptotic regime where $\alpha \to \infty$ and $N_{\mathsf{RF}} = \lceil p\alpha \rceil$ with p > 0 a constant. Then,

$$\sum_{\ell < N_{\mathsf{RF}}} \lambda_{\ell}(\mathcal{B}_{\alpha}) = \min(p, 1)\alpha + o(\alpha), \tag{53}$$

which (see App. B) is a consequence of (52). Therefore,

$$\sum_{\ell < N_{\mathsf{RF}}} \lambda_{\ell}(\mathcal{B}_{\alpha}) = \alpha + o(\alpha) \tag{54}$$

if $p \ge 1$. Recalling the squint-free condition in (50), this implies that, asymptotically, α RF chains are needed to approach squint-free performance.

D. Beamspace Architecture

An instance of the above general ULA result had been empirically observed in the context of beamspace MIMO [27], namely that the beam squint can be mitigated with $N_{\rm RF} \approx \alpha$ RF chains and a simple analog network. The ℓ th column of $W_{\rm a}$ is then the MRT beamformer $\frac{a(f_\ell)}{\sqrt{N}}$ for the relative frequency

$$f_{\ell} = \frac{c}{u_{x}d_{x}} \cdot \frac{\ell - \frac{N_{\text{RF}} - 1}{2}}{N} = \frac{\ell - \frac{N_{\text{RF}} - 1}{2}}{\alpha}W,$$
 (55)

such that W is segregated into $N_{\rm RF}$ subbands spaced by $\frac{W}{\alpha}$. Intuitively, this narrower subbands are less susceptible to beam squint; in fact, they are dimensioned such that the loss in beamforming gain is (asymptotically) about 3 dB, with the digital stage correcting this residual loss.²

A dual interpretation, recalling (23), is that the ℓ th analog beamformer points (at its own central frequency) in direction $(1+\frac{f_\ell}{f_c})u_x$. At the analog stage, we are therefore faced with a bank of beams arranged regularly in u_x , hence the beamspace denomination.

As the columns are orthonormal, (34) gives

$$\frac{g_{\mathsf{avg}}}{N} = \frac{1}{NW} \int_{-\frac{W}{2}}^{\frac{W}{2}} \|\boldsymbol{a}^*(f)\boldsymbol{W}_{\mathsf{a}}\|^2 df \tag{56}$$

$$= \sum_{\ell \le N_{\text{PE}}} \frac{1}{W} \int_{-\frac{W}{2}}^{\frac{W}{2}} \frac{|\boldsymbol{a}^*(f)\boldsymbol{a}(f_{\ell})|^2}{N^2} df.$$
 (57)

 2 Precisely, the maximum loss at the subband boundaries is 3.92 dB for $\alpha=1$, which follows from ${\rm sinc}^2(1/2)=\frac{4}{\pi^2}\approx 0.405$.

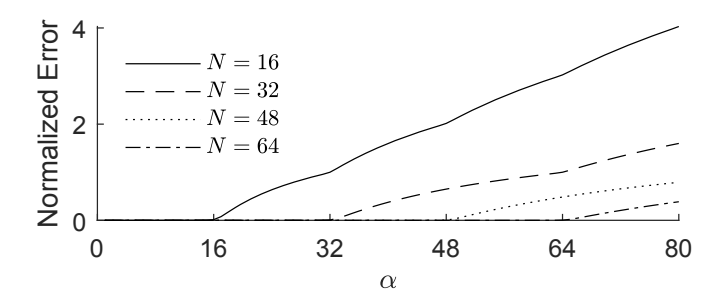


Fig. 3. Validity of the continuous-aperture representation.

To again move into the continuous-aperture realm, we let $N \to \infty$ while retaining the aperture, whereby

$$\frac{|\boldsymbol{a}^*(f)\boldsymbol{a}(f_{\ell})|^2}{N^2} = \left(\frac{\sin\left(\pi\left(\ell - \frac{N_{\mathsf{RF}} - 1}{2} - \frac{f}{W}\alpha\right)\right)}{N\sin\left(\pi\left(\ell - \frac{N_{\mathsf{RF}} - 1}{2} - \frac{f}{W}\alpha\right)/N\right)}\right)^2$$

$$\rightarrow \operatorname{sinc}^2\left(\ell - \frac{N_{\mathsf{RF}} - 1}{2} - \frac{f}{W}\alpha\right) \tag{58}$$

and

$$\frac{g_{\text{avg}}}{N} \to \sum_{\ell < N_{\text{RF}}} \frac{1}{W} \int_{-\frac{W}{2}}^{\frac{W}{2}} \operatorname{sinc}^{2} \left(\ell - \frac{N_{\text{RF}} - 1}{2} - \frac{f}{W}\alpha\right) df$$

$$= \frac{1}{\alpha} \sum_{\ell < N_{\text{DF}}} \int_{\ell - \frac{N_{\text{RF}} - 1}{2} - \frac{\alpha}{2}}^{\ell - \frac{N_{\text{RF}} - 1}{2} - \frac{\alpha}{2}} \operatorname{sinc}^{2} t \, dt \tag{59}$$

Let us again consider the asymptotic regime, $\alpha \to \infty$ and $N_{\rm RF} = \lceil p\alpha \rceil$ with p>0 a constant. It is shown in App. C that (59) converges to $\min(p,1)$. The result is thus identical to its counterpart—recall (53)—with the optimum eigenvectors, demonstrating the asymptotic optimality of the beamspace architecture. This architecture is computationally efficient and compelling in that no amplitude tapering is required. On top of that, the normalized response at the ℓ th RF chain, given in (58), concentrates around f_ℓ such that having a much smaller bandwidth at each RF chain incurs negligible loss. With a bandwidth of $\frac{2}{\alpha}W$ per RF chain—precisely, between $f_\ell - \frac{W}{\alpha}$ and $f_\ell + \frac{W}{\alpha}$ —the normalized average beamforming gain becomes

$$\left(\int_{-1}^{1} \operatorname{sinc}^{2} t \, dt\right) \min(p, 1) \approx 0.902 \min(p, 1) \tag{60}$$

which falls short by only 0.45 dB. Doubling the bandwidth per RF chain shrinks this deficit to 0.22 dB.

E. Remarks

The analysis in this section entails two limits, infinitesimal element spacing and infinite aperture-bandwidth product, and care should be exercised to ensure the relevance to regimes of interest [38].

Recalling (49), Fig. 3 depicts the normalized approximation error for the first limit³

$$\frac{\sum_{\ell} \left(\frac{\alpha}{N} \lambda_{\ell}(\boldsymbol{B}) - \lambda_{\ell}(\mathcal{B}_{\alpha})\right)^{2}}{\sum_{\ell} \lambda_{\ell}^{2}(\mathcal{B}_{\alpha})}.$$
 (61)

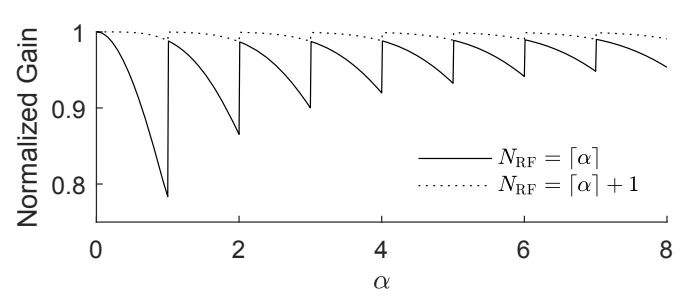


Fig. 4. Normalized gain with respect to α . The sawtooth behavior, caused by the ceiling function on the number of RF chains, quickly abates.

The figure evidences that the continuous-aperture representation is fully valid provided that $\alpha \leq N$, a condition clearly fulfilled for any scenario of interest because

$$\alpha = N \frac{W}{f_c} \frac{d_x u_x}{\lambda} \ll N. \tag{62}$$

This leaves the second limit, base on which the analysis is valid as long as α is minimally large. Pleasingly, even for very small α this turns out to be the case. Fig. 4 depicts the normalized gain $\left(\sum_{\ell < N_{\rm RF}} \lambda_{\ell}(\mathcal{B}_{\alpha})\right)/\alpha$ with respect to α , confirming that, for virtually any α , squint-free performance can be virtually achieved with $\lceil \alpha \rceil + 1$ RF chains.

VI. PLANAR ARRAYS

The generalization to planar arrays is not straightforward in that a naive separable architecture makes an inefficient use of the RF chains. For planar arrays, the intensity of beam squint can be measured by

$$\alpha \equiv \begin{bmatrix} \alpha_x \\ \alpha_y \end{bmatrix} = \frac{W}{f_c} \begin{bmatrix} \frac{L_x u_x}{\lambda} \\ \frac{L_y u_y}{\lambda} \end{bmatrix}, \tag{63}$$

which is a natural extension of α for linear arrays.

A. Separable Architecture

Motivated by (5), separable beamformers are often considered where [9, Ch. 1.2]

$$\mathbf{W}_{\mathsf{a}} = \mathbf{W}_x \otimes \mathbf{W}_y \tag{64}$$

with $W_x \in \mathbb{C}^{N_x \times N_{\mathrm{RF},x}}$ and $W_y \in \mathbb{C}^{N_y \times N_{\mathrm{RF},y}}$, and with $N_{\mathrm{RF}} = N_{\mathrm{RF},x} N_{\mathrm{RF},y}$. Then,

$$g(f) = \| \left((\boldsymbol{W}_{x}^{*} \otimes \boldsymbol{W}_{y}^{*}) (\boldsymbol{W}_{x} \otimes \boldsymbol{W}_{y}) \right)^{-\frac{1}{2}} \cdot (\boldsymbol{W}_{x}^{*} \otimes \boldsymbol{W}_{y}^{*}) (\boldsymbol{a}_{x}(f) \otimes \boldsymbol{a}_{y}(f)) \|^{2}$$
(65)

$$= \| (\boldsymbol{W}_{x}^{*} \boldsymbol{W}_{x})^{-\frac{1}{2}} \boldsymbol{W}_{x}^{*} \boldsymbol{a}_{x}(f)$$

$$\otimes (\boldsymbol{W}_{y}^{*} \boldsymbol{W}_{y})^{-\frac{1}{2}} \boldsymbol{W}_{y}^{*} \boldsymbol{a}_{y}(f) \|^{2}$$
(66)

$$= \| (\boldsymbol{W}_{x}^{*} \boldsymbol{W}_{x})^{-\frac{1}{2}} \boldsymbol{W}_{x}^{*} \boldsymbol{a}_{x}(f) \|^{2}$$

$$\cdot \| (\boldsymbol{W}_{x}^{*} \boldsymbol{W}_{y})^{-\frac{1}{2}} \boldsymbol{W}_{y}^{*} \boldsymbol{a}_{y}(f) \|^{2}$$
(67)

$$=g_x(f)g_y(f) \tag{68}$$

given

$$g_x(f) = \|(\mathbf{W}_x^* \mathbf{W}_x)^{-\frac{1}{2}} \mathbf{W}_x^* \mathbf{a}_x(f)\|^2$$
 (69)

$$g_y(f) = \|(\mathbf{W}_y^* \mathbf{W}_y)^{-\frac{1}{2}} \mathbf{W}_y^* \mathbf{a}_y(f)\|^2.$$
 (70)

 $^{^3\}lambda_\ell(\mathcal{B}_\alpha)$ can be computed via the software package chebfun2 [39].

It follows that (see App. D)

$$\frac{g_{\mathsf{avg}}}{N} \le \min\left(\frac{g_{\mathsf{avg},x}}{N_x}, \frac{g_{\mathsf{avg},y}}{N_y}\right) \tag{71}$$

where $g_{\mathsf{avg},x} = \frac{1}{W} \int_{-\frac{W}{2}}^{\frac{W}{2}} g_x(f) df$ and $g_{\mathsf{avg},y} = \frac{1}{W} \int_{-\frac{W}{2}}^{\frac{W}{2}} g_y(f) df$. Attaining $g_{\mathsf{avg}} \approx N$ with a separable beamforming structure

Attaining $g_{\text{avg}} \approx N$ with a separable beamforming structure entails $g_{\text{avg},x} \approx N_x$ and $g_{\text{avg},y} \approx N_y$. For $u_x \neq 0$ and $u_y \neq 0$, asymptotically in the array aperture and/or the bandwidth it holds that $N_{\text{RF},x} \geq \alpha_x$ and $N_{\text{RF},y} \geq \alpha_y$ as per Sec. V. Thus,

$$N_{\mathsf{RF}} \ge \alpha_x \alpha_y = \frac{L_x L_y u_x u_y}{c^2} W^2,\tag{72}$$

which is *quadratic* in the diagonal dimensions of the array and also quadratic in the bandwidth. In the sequel, it is shown that a nonseparable beamformer can greatly reduce such N_{RF} .

B. Continuous-Aperture Representation

Again resorting to a continuous-aperture representation, the counterpart to \boldsymbol{B} is the integral operator

$$\mathcal{B}_{\alpha} : L^{2}(\mathbb{R}^{2}) \to L^{2}(\mathbb{R}^{2})$$

$$s(\mathbf{r}) \mapsto \int B_{\alpha}(\mathbf{r}', \mathbf{r}) s(\mathbf{r}) d\mathbf{r}$$
(73)

where

$$B_{\alpha}(\mathbf{r}', \mathbf{r}) = \|\alpha\| \operatorname{sinc}(\pi \alpha^{\top} (\mathbf{r} - \mathbf{r}')) [\mathbf{r} \in I^{2}] [\mathbf{r}' \in I^{2}]$$
 (74)

is the kernel. The matrix B can again be recovered from (74) by sampling at the normalized element coordinates, precisely

$$[\boldsymbol{B}]_{n',n} = \frac{1}{\|\boldsymbol{\alpha}\|} B_{\boldsymbol{\alpha}} \left(\begin{bmatrix} \frac{x_{n'}}{L_x} \\ \frac{y_{n'}}{L_y} \end{bmatrix}, \begin{bmatrix} \frac{x_n}{L_x} \\ \frac{y_n}{L_y} \end{bmatrix} \right). \tag{75}$$

In terms of eigenvalues, the continuous representation becomes exact as the spacings vanish, namely [34, Sec. V-C]

$$\frac{\|\boldsymbol{\alpha}\|}{N}\lambda_{\ell}(\boldsymbol{B}) \to \lambda_{\ell}(\mathcal{B}_{\boldsymbol{\alpha}}) \tag{76}$$

in two-norm as N_x and N_y grow large with a fixed ratio. The squint-free condition is

$$\sum_{\ell < N_{\mathsf{RF}}} \lambda_{\ell}(\mathcal{B}_{\alpha}) \approx \|\alpha\|. \tag{77}$$

C. A Bag of Tricks

The operator \mathcal{B} obtained from the continuous-aperture representation is still ill-suited to analysis. To enable further progress, some handy results are set forth in this subsection that allow capitalizing on ULAs asymptotics.

Let us construct a rotation matrix $\mathbf{R} \in \mathbb{R}^{2\times 2}$ whose first row is $\frac{\alpha}{\|\alpha\|}$, and then rotate the axes into

$$\tilde{\boldsymbol{r}} = \begin{bmatrix} \tilde{r}_x & \tilde{r}_y \end{bmatrix}^{\top} = \boldsymbol{R}\boldsymbol{r}$$
 $\tilde{\boldsymbol{r}}' = \begin{bmatrix} \tilde{r}'_x & \tilde{r}'_y \end{bmatrix} = \boldsymbol{R}\boldsymbol{r}'.$ (78)

The right-hand side of (74) can then be recast as

$$\|\boldsymbol{\alpha}\|\operatorname{sinc}(\boldsymbol{\pi}\|\boldsymbol{\alpha}\|(\tilde{r}_x - \tilde{r}_x'))[\tilde{\boldsymbol{r}} \in \boldsymbol{R}I^2][\tilde{\boldsymbol{r}}' \in \boldsymbol{R}I^2].$$
 (79)

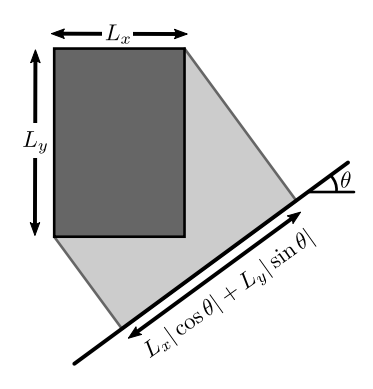


Fig. 5. Projection of the UPA onto the line parallel to $[\cos \theta \quad \sin \theta]^{\top}$.

Defining the kernel

$$\tilde{B}_{\alpha}(\tilde{r}'_{x}, \tilde{r}_{x}) = \|\alpha\|\operatorname{sinc}(\pi\|\alpha\|(\tilde{r}_{x} - \tilde{r}'_{x}))$$

$$\cdot \left(\int \left[\tilde{r} \in \mathbf{R}I^{2}\right] d\tilde{r}_{y}\right)^{1/2} \left(\int \left[\tilde{r}' \in \mathbf{R}I^{2}\right] d\tilde{r}'_{y}\right)^{1/2}$$
(80)

and the corresponding operator $\tilde{\mathcal{B}}_{\alpha}: L^2(\mathbb{R}) \to L^2(\mathbb{R})$, it is shown in App. E that the eigenvalues of $\tilde{\mathcal{B}}_{\alpha}$ and \mathcal{B}_{α} coincide. If the factors

$$\left(\int \left[\tilde{\boldsymbol{r}} \in \boldsymbol{R} I^2\right] d\tilde{r}_y\right)^{1/2} \qquad \left(\int \left[\tilde{\boldsymbol{r}}' \in \boldsymbol{R} I^2\right] d\tilde{r}_y'\right)^{1/2} \tag{81}$$

are replaced by indicator functions, the above boils down to the ULA kernel. This motivates bounding these factors with scalar multiples of the indicator function and invoking the Courant min-max theorem. Precisely, $\int \left[\tilde{r} \in RI^2\right] d\tilde{r}_y$ is a piecewise linear function connecting the points

$$(-L_1/2,0), (-L_2/2,L_3), (L_2/2,L_3), (L_1/2,0)$$
 (82)

given

$$L_1 = \frac{|\alpha_x| + |\alpha_y|}{\|\boldsymbol{\alpha}\|} \tag{83}$$

$$L_2 = \frac{\left| |\alpha_x| - |\alpha_y| \right|}{\|\boldsymbol{\alpha}\|} \tag{84}$$

$$L_3 = \frac{\|\boldsymbol{\alpha}\|}{\max(|\alpha_x|, |\alpha_y|)} \tag{85}$$

Also.

$$\delta L_3 \left[\tilde{r}_x \in ((1 - \delta)L_1 + \delta L_2)I \right]$$

$$\leq \int \left[\tilde{r} \in \mathbf{R}I^2 \right] d\tilde{r}_y \leq L_3 \left[\tilde{r}_x \in L_1 I \right]$$
 (86)

where $\delta \in [0, 1]$ is a constant to be determined.

Using (86) and the fact that \mathcal{B} and $\tilde{\mathcal{B}}$ share the same eigenvalues, it is shown in App. F that

$$\delta L_3 \lambda_{\ell}(\mathcal{B}_{\alpha^{\text{lo}}}) \le \lambda_{\ell}(\mathcal{B}_{\alpha}) \le L_3 \lambda_{\ell}(\mathcal{B}_{\alpha^{\text{up}}}),$$
 (87)

where

$$\alpha^{\mathsf{lo}} \equiv \|\boldsymbol{\alpha}\| \left((1 - \delta)L_1 + \delta L_2 \right) \tag{88}$$

$$\alpha^{\mathsf{up}} \equiv \|\boldsymbol{\alpha}\| L_1. \tag{89}$$

TABLE II
NORMALIZED AVERAGE BEAMFORMING GAIN (WORST VALUE OVER AZIMUTH ANGLE) FOR VARIOUS SETUPS

	# additional Bandwidth [GHz]										
	RF chains	1	2	3	4	5	10	15	20	25	30
Optimal	0	0.9877	0.9523	0.8984	0.8324	0.9776	0.9638	0.9680	0.9720	0.9737	0.9749
	1	1.0000	0.9993	0.9967	0.9933	0.9991	0.9961	0.9959	0.9961	0.9960	0.9959
	2	1.0000	0.9999	0.9999	0.9998	0.9998	0.9996	0.9996	0.9995	0.9994	0.9993
Beamspace	0	0.9876	0.9518	0.8963	0.8266	0.9089	0.9308	0.9431	0.9510	0.9564	0.9603
	1	0.8170	0.8349	0.8600	0.8868	0.9264	0.9405	0.9492	0.9551	0.9596	0.9631
	2	0.9952	0.9819	0.9632	0.9433	0.9531	0.9607	0.9658	0.9695	0.9722	0.9744

D. Number of Required RF Chains

Consider a bandwidth r_1W and an aperture $r_2L_x \times r_2L_y$ where $r_1, r_2 > 0$ are constants. Then,

$$\alpha = \frac{rW}{f_{\rm c}} \begin{bmatrix} \frac{L_x u_x}{\lambda} \\ \frac{L_y u_y}{\lambda} \end{bmatrix}$$
 (90)

depends on $r \equiv r_1 r_2$, not individually on r_1 and r_2 . With the number of RF chains at

$$N_{\mathsf{RF}} = [p\alpha^{\mathsf{up}}],$$
 (91)

let us once more consider the asymptotic regime, via $r\to\infty$. Armed with (87), it is shown in App. G that the no-squint condition

$$\sum_{\ell < N_{\text{DE}}} \lambda_{\ell}(\mathcal{B}) = \|\boldsymbol{\alpha}\| + o(r) \tag{92}$$

holds if and only if $p \ge 1$. The minimum number of RF chains that asymptotically attain squint-free performance is thus

$$\alpha^{\mathsf{up}} = |\alpha_x| + |\alpha_y| \tag{93}$$

$$= \frac{W}{f_c} \cdot \frac{L_x |\cos \theta| + L_y |\sin \theta|}{\lambda} \sin \phi, \tag{94}$$

where $L_x |\cos \theta| + L_y |\sin \theta|$ is the projection of the UPA onto a line parallel to $[\cos \theta \ \sin \theta]^{\mathsf{T}}$ (see Fig. 5). In conjunction with $\sin \phi$, this projects the array onto the direction of beamforming as illustrated in Fig. 1.

This result can be readily generalized to non-UPA planar topologies.

E. Beamspace Architecture

A beamspace architecture analogous to the ULA one in Sec. V-D can be constructed by choosing the ℓ th column of W_a as the MRT beamformer $a(f_\ell)$ for relative frequency

$$f_{\ell} = \frac{\ell - \frac{N_{\mathsf{RF}} - 1}{2}}{\alpha^{\mathsf{up}}} W. \tag{95}$$

However, as the columns of W_a are no longer orthonormal, the proof set forth for linear arrays does not carry over to show that (94) holds for planar beamspace arrays. Results in the next section support this, yet the proof is still open.

VII. NUMERICAL RESULTS

This section presents additional results supporting the relevance of the asymptotic analysis to values of interest, not only for future 6G or WiFi systems, but even for current 5G deployments.

As an embodiment of the arrays that may be featured in future systems, a 128×128 UPA with half-wavelength spacing is postulated; it would occupy only 6.4 cm \times 6.4 cm at $f_{\rm c} = 300$ GHz. From (63), α depends on the product $W \sin \phi$. Without loss of generality we can thus fix $\phi = 90^{\circ}$ and sweep only W. From (94), the highest value over azimuth of $\alpha^{\rm up}$ is

$$\alpha^{\mathsf{up}} = \frac{W}{f_c} \sqrt{L_x^2 + L_y^2} / \lambda. \tag{96}$$

For a bandwidth of W=1 GHz at $f_c=300$ GHz, this equals $\frac{1 \, \mathrm{GHz}}{300 \, \mathrm{GHz}} \times 64 \sqrt{2} \approx 0.302$; as it is proportional to W, it can be readily scaled for other bandwidths or carrier frequencies. Table II lists the average beamforming gain normalized by its squint-free counterpart, $\frac{g_{\mathrm{avg}}}{N}$, for the optimal and beamspace architectures; precisely, the listed values are the worst (over azimuth) normalized gains. The number of additional RF chains in the table is $N_{\mathrm{RF}} - \lceil \alpha^{\mathrm{up}} \rceil$. For the optimal architecture, $\lceil \alpha^{\mathrm{up}} \rceil + 1$ RF chains ensure over 99% of the squint-free gain over the entire range and, for strong squints, $\lceil \alpha^{\mathrm{up}} \rceil$ RF chains suffice to perform almost as impressively. As of the beamspace architecture, it exhibits a remarkably small performance deficit relative to the optimal one—a deficit that can be overcome with only one or two extra RF chains. Given its simplicity, this makes it a decidedly attractive alternative.

Turning to 5G, a 16×16 UPA is a typical array structure; it occupies $8 \text{ cm} \times 8 \text{ cm}$ at 30 GHz. Its performance can also be read from Table II by virtue of the fact that only the product between the aperture and the normalized bandwidth matters. Precisely, the performance for $\{0.8, 1.6, 2.4, 3.2, 4.0\}$ GHz of bandwidth at $f_c = 30$ GHz is given by the values listed under $\{1, 2, 3, 4, 5\}$ GHz in the table. The same observations made for the larger array at $f_c = 300$ GHz therefore apply, and they further do for any other combination of aperture, bandwidth, and carrier frequency that falls within the scope of this table.

VIII. EXTENSIONS

While the formulation hitherto has considered a general hybrid array, fully-connected as per the illustration in Fig. 6, this section turns the attention to the more restrictive hybridly-connected and partially-connected structures, and further to receivers equipped themselves with an array.

A. Hybridly-Connected Architecture

In a hybridly-connected architecture (see Fig. 6), the array is partitioned into subarrays and only a subset of the RF chains is connected to each subarray [40]. With proper antenna

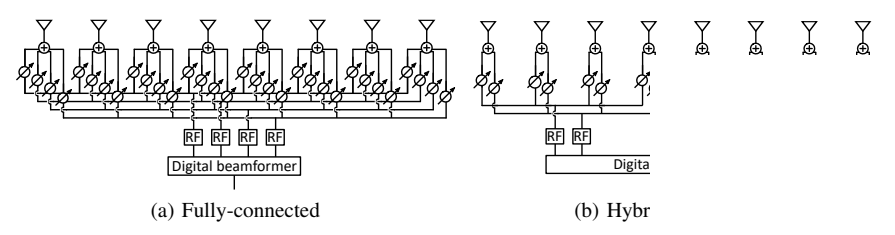


Fig. 6. Hybrid architectures: fully-connected, hybridly-connected, and partial

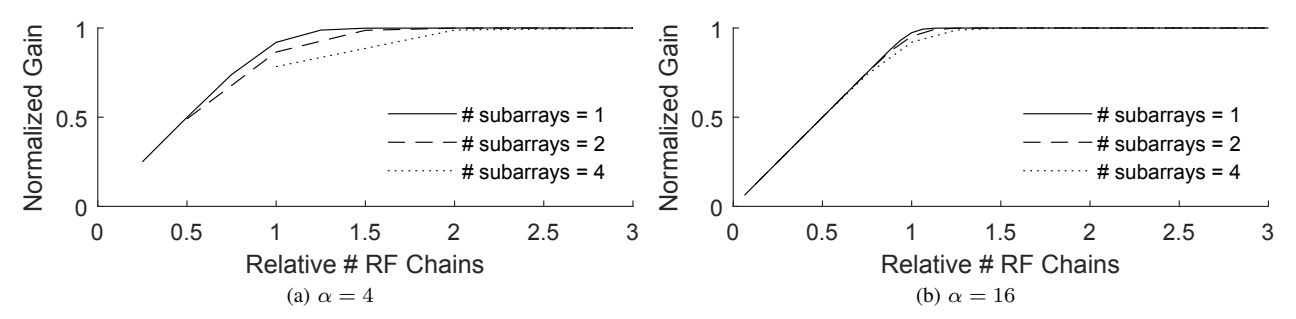


Fig. 7. Normalized beamforming gain $\frac{g_{avg}}{N}$ for a 128-element ULA. The analog beamformer maximizing the average beamforming gain is used. The relative number of RF chains for the horizontal axis is the number of RF chains normalized by the number of required RF chains, that is, $\frac{N_{RE}}{\alpha}$.

indexing, the analog beamforming matrix exhibits a block diagonal structure, namely

$$\mathbf{W}_{\mathsf{a}} = \mathsf{blkdiag}(\mathbf{W}_{\mathsf{a},0}, \dots, \mathbf{W}_{\mathsf{a},M-1})$$
 (97)

with $W_{a,m}$ the analog beamformer for the mth subarray and M the number of subarrays. Plugging (97) into (12) gives

$$g(f) = \|\mathbf{a}^{*}(f) \text{blkdiag}(\mathbf{W}_{\mathsf{a},0}(\mathbf{W}_{\mathsf{a},0}^{*}\mathbf{W}_{\mathsf{a},0})^{-\frac{1}{2}}, \dots, \mathbf{W}_{\mathsf{a},M-1}(\mathbf{W}_{\mathsf{a},M-1}^{*}\mathbf{W}_{\mathsf{a},M-1})^{-\frac{1}{2}})\|^{2}$$
(98)
$$= \sum g_{m}(f)$$
(99)

where

$$g_m(f) = \|\boldsymbol{a}_m^*(f)\boldsymbol{W}_{\mathsf{a},m}(\boldsymbol{W}_{\mathsf{a},m}^*\boldsymbol{W}_{\mathsf{a},m})^{-\frac{1}{2}}\|^2$$
 (100)

given $a_m(f)$ as the channel for the mth subarray. Therefore,

$$g_{\text{avg}} = \sum_{m} g_{\text{avg},m} \tag{101}$$

where

$$g_{\mathsf{avg},m} = \frac{1}{W} \int_{-\frac{W}{2}}^{\frac{W}{2}} g_m(f) df.$$
 (102)

The behavior of a hybridly-connected array can thus be broken down into that of the subarrays, and the squint-free criterion is $g_{avg,m}$ approximately equaling the number of elements in the mth subarray for every m.

Let us first consider an N-element ULA composed of M subarrays in the asymptotic regime. Each subarray is connected to $\frac{N_{\rm RF}}{M}$ RF chains. From Sec. V, squint-free performance requires

$$\frac{N_{\mathsf{RF}}}{M} \ge \frac{\alpha}{M} \Leftrightarrow N_{\mathsf{RF}} \ge \alpha, \tag{103}$$

as in the fully-connected architecture. This is remarkable given the M-fold savings in number of phase shifters, yet

the asymptotic regime is now determined by $\frac{\alpha}{M} \to \infty$, whose convergence rate is slower (see Fig. 7).

The situation changes with planar arrays. Let us consider an $N_x \times N_y$ UPA composed of $M_x \times M_y$ subarrays. The asymptotic regime of interest is the one considered in Sec. VI with fixed M_x and M_y . Each subarray is then connected to $\frac{N_{\rm RF}}{M_x M_y}$ RF chains. Attaining squint-free performance requires

$$\frac{N_{\mathsf{RF}}}{M_x M_y} \ge \frac{|\alpha_x|}{M_x} + \frac{|\alpha_y|}{M_y} \Leftrightarrow N_{\mathsf{RF}} \ge M_y |\alpha_x| + M_x |\alpha_y|, \tag{104}$$

which is at least $min(M_x, M_y)$ times larger than the number of RF chains required by the fully-connected case.

B. Partially-Connected Architecture

With a single RF chain per subarray, a partially-connected array is the simplest instance of a hybridly-connected architecture (see Fig. 6). As per (101), the behavior of a hybrid array with a partially-connected analog network can be decomposed into that of the subarrays.

Consider an N-element ULA composed of $M=N_{\rm RF}$ subarrays with identical subarray beamformer ${\boldsymbol w}_{\rm a}\in \mathbb{C}^{\frac{N}{M}}$. As per (101), $g_{\rm avg}=Mg_{\rm avg,0}$. Two subarray beamformers are considered, the MRT beamformer and the optimal beamformer, both implementable with a single RF chain and M delay lines (see App. H).

· For the MRT beamformer,

$$g_{\text{avg}} = \frac{M}{W} \int_{-\frac{W}{2}}^{\frac{W}{2}} F_{\frac{N}{M}} \left(\frac{2\pi d_x u_x}{c} f \right) df$$
 (105)

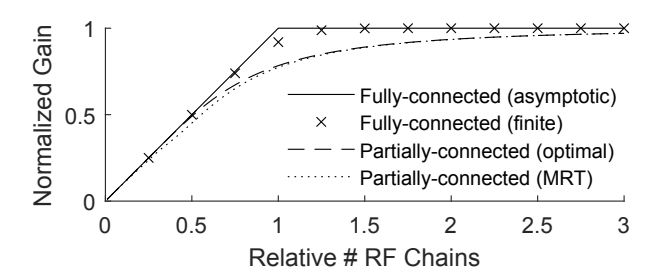


Fig. 8. Comparison of array architectures. For the fully-connected architecture, $\alpha\to\infty$ and $\alpha=4$ are considered. The relative number of RF chains for the horizontal axis is the number of RF chains normalized by the number of required RF chains, that is, $\frac{N_{\rm RF}}{\alpha}$. This equals $\frac{M}{\alpha}$ for partially-connected architectures.

and thus

$$\frac{g_{\text{avg}}}{N} \to \frac{1}{W} \int_{-\frac{W}{2}}^{\frac{W}{2}} \operatorname{sinc}^{2} \left(\frac{L_{x} u_{x}}{M c} f\right) df \tag{106}$$

$$= \frac{M}{\alpha} \int_{-\frac{\alpha}{2M}}^{\frac{\alpha}{2M}} \operatorname{sinc}^2 t \, dt \tag{107}$$

$$= \frac{2M}{\pi\alpha} \operatorname{Si}\left(\frac{\pi\alpha}{M}\right) - \operatorname{sinc}^2 \frac{\alpha}{2M}$$
 (108)

as the array densifies; here, $Si(\cdot)$ is the sine integral.

For the optimal beamformer in terms of average beamforming gain, recalling (49),

$$\frac{g_{\text{avg}}}{N} \to \frac{\lambda_0(\mathcal{B}_{\alpha/M})}{\alpha/M} \tag{109}$$

as array densifies.

For growing α , both (108) and (109) expand as

$$\frac{M}{\alpha} + \mathcal{O}\left(\frac{M}{\alpha}\right). \tag{110}$$

Compared in Fig. 8 are the normalized average beamforming gains for fully- and partially-connected architectures. Recalling (53), the asymptotic result $\min(p,1)$ is plotted for the fully-connected architecture while (108) and (109) are plotted for the partially-connected architecture. In accordance with (110), the slope of all of those curves at zero is 1. Thus, in the regime where the squint is decidedly too high to compensate, fully-connected and partially-connected architectures perform identically in terms of average array gain.

Although the squint cannot be completely eradicated with a partially-connected architecture, the latter is rather enticing because of the M-fold saving in number of phase shifters. For instance, with $M=\alpha,2\alpha,3\alpha$, a partially-connected architecture incurs respective losses of only 1.11, 0.29, 0.13 dB, even with simple MRT beamforming; in Fig. 8, these losses can be appreciated in linear scale. At the expense of a small loss in beamforming gain, then, only 1/M as many phase shifters are required, with the ensuing benefits in terms of cost and power consumption. For any acceptable loss, the values of M in a partially-connected structure could be optimized on the basis of the respective costs and power consumptions of an analog phase shifter and a complete RF chain [41]–[43].

Similar to their hybridly-connected brethren, partially-connected architectures become less alluring with planar arrays. To maintain the subarray size, one needs the scalings

$$M_x \propto \alpha_x \qquad M_y \propto \alpha_y,$$
 (111)

whereby the substantial disadvantage of the separable architecture in Sec. VI-A is reproduced. This shortcoming can be alleviated by a use of dynamic subarrays [32], at the expense of additional hardware complexity.

C. Multiantenna Receiver

The separable property of far-field LOS multiantenna channels enables the extension to such a setting too. Positing an $N_{\rm t}$ -element transmitter and an $N_{\rm r}$ -element receiver, the LOS channel can be expressed as [44, Sec. II-A]

$$\boldsymbol{H}(f) = \boldsymbol{a}_{\mathrm{r}}(f)\boldsymbol{a}_{\mathrm{t}}^{*}(f) \tag{112}$$

where $a_{\rm t}(f) \in \mathbb{C}^{N_{\rm t}}$ is the normalized channel between the transmit array and the receive array center, and reciprocally for $a_{\rm r}(f) \in \mathbb{C}^{N_{\rm r}}$. The squint-free condition is $g_{\rm avg} \approx N_{\rm t} N_{\rm r}$.

Let us denote the analog and digital beamformers by $W_{\rm a,t}$ and $w_{\rm d,t}(f)$ for the transmitter, and $W_{\rm a,r}$ and $w_{\rm d,r}(f)$ for the receiver. An analogous signal model to that in Sec. II-C is

$$y(f) = \boldsymbol{w}_{d,r}^*(f) \boldsymbol{W}_{a,r}^* [\boldsymbol{H}(f) \boldsymbol{W}_{a,t} \boldsymbol{w}_{d,t}(f) s(f) + \boldsymbol{v}(f)]$$
(113)

where each entry of v(f) describes a white Gaussian noise process with unit power spectral density. Letting s(f) have unit power, the power constraint becomes

$$\frac{1}{W} \int_{-\frac{W}{2}}^{\frac{W}{2}} \| \boldsymbol{W}_{\mathsf{a},\mathsf{t}} \boldsymbol{w}_{\mathsf{d},\mathsf{t}}(f) \|^2 df = \mathsf{SNR}. \tag{114}$$

Also, without loss of generality, we let $\|\mathbf{W}_{a,r}\mathbf{w}_{d,r}(f)\| = 1$. Replicating the simplifications in Sec. II-C gives

$$y(f) = \sqrt{g(f)p(f)}s(f) + \boldsymbol{W}_{a,r}^*\boldsymbol{w}_{d,r}^*(f)\boldsymbol{v}(f)$$
(115)

where

$$g(f) = \|\boldsymbol{w}_{d,r}^*(f)\boldsymbol{W}_{a,r}^*\boldsymbol{H}(f)\boldsymbol{W}_{a,t}\boldsymbol{w}_{d,t}(f)\|^2$$
(116)

$$= |a_{t}^{*}(f)W_{a,t}w_{d,t}(f)|^{2} \cdot |a_{r}^{*}(f)W_{a,r}w_{d,r}(f)|^{2}$$
(117)

$$= q_{\mathbf{t}}(f)q_{\mathbf{r}}(f) \tag{118}$$

with

$$g_{t}(f) = |\boldsymbol{a}_{t}^{*}(f)\boldsymbol{W}_{\mathsf{a},t}\boldsymbol{w}_{\mathsf{d},t}(f)|^{2}$$
(119)

$$g_{\mathbf{r}}(f) = |\boldsymbol{a}_{\mathbf{r}}^{*}(f)\boldsymbol{W}_{\mathsf{a},\mathbf{r}}\boldsymbol{w}_{\mathsf{d},\mathbf{r}}(f)|^{2}. \tag{120}$$

The effective noise $W_{\rm a,r}^* w_{\rm d,r}^*(f) v(f)$ is a white Gaussian process with unit power spectral density.

Recalling the definition of average beamforming gain in (32), it is shown in App. D that

$$\frac{g_{\mathsf{avg},t}}{N_{\mathsf{t}}} + \frac{g_{\mathsf{avg},r}}{N_{\mathsf{t}}} - 1 \le \frac{g_{\mathsf{avg}}}{N_{\mathsf{t}}N_{\mathsf{r}}} \le \min \left(\frac{g_{\mathsf{avg},\mathsf{t}}}{N_{\mathsf{t}}}, \frac{g_{\mathsf{avg},\mathsf{r}}}{N_{\mathsf{t}}} \right) . \tag{121}$$

From this result, plus $g_{\rm avg,t} \leq N_{\rm t}$ and $g_{\rm avg,r} \leq N_{\rm r}$, it follows that

$$\frac{g_{\rm avg,t}}{N_{\rm t}} = \frac{g_{\rm avg,r}}{N_{\rm r}} = 1 \tag{122}$$

TABLE III SUMMARY

	Partially-connected	Hybridly-connected	Fully-connected
Property in terms of squint	Essentially identical to an analog array whose size equals that of subarray	Essentially identical to a fully-connected hybrid array whose size equals that of subarray	-
# of phase shifters	N	$rac{N_{RF}N}{M_xM_y}$	$N_{RF}N$
# of required RF chains (linear) # of required RF chains (planar)	* - * -	$ lpha_x \ M_y lpha_x + M_x lpha_y ^\dagger$	$\frac{ \alpha_x }{ \alpha_x + \alpha_y ^{\dagger}}$

^{*} Partially-connected architecture cannot enjoy squint-free performance.

 $^{^\}dagger$ The results for linear and planar arrays are consistent; linear array is a special case of planar array with $lpha_y=0$.

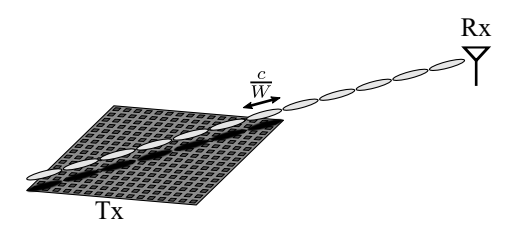


Fig. 9. A train of symbols, each of spatial length $\frac{c}{W}$, traveling over the array along the worst possible direction in terms of delay across elements.

is a necessary and sufficient condition for

$$\frac{g_{\text{avg}}}{N_t N_r} = 1. \tag{123}$$

This implies that both $g_{\text{avg},t} \approx N_{\text{t}}$ and $g_{\text{avg},r} \approx N_{\text{r}}$ are needed to ensure $g_{\text{avg}} \approx N_{\text{t}} N_{\text{r}}$, and vice versa, whereby the multiantenna problem is seen to decouple into two problems that have already been addressed.

IX. CONCLUSION

The main takeaway point of this work is that hybrid arrays can operate free of beam squint, just like digital arrays, only with a much smaller number of RF chains. Although derived asymptotically in the bandwidth-aperture product, this result applies for virtually any value of that product.

For a hybrid linear array meant to beamform in any direction, the needed number of RF chains is $\frac{1}{c}WL$. In contrast, a digital array requires a chain per antenna element, which for half-wavelength element spacing amounts to $\frac{L}{\lambda/2} = \frac{2}{c}f_cL$. The contrast between the two expressions evidences something fundamental, namely that it is the bandwidth rather than the carrier frequency that matters to the beam squint. Indeed, $\frac{c}{W}$ is roughly the spatial length of a symbol, and squint arises once symbols cease to be much longer than the array (see Fig. 9). The value $\frac{1}{c}WL$ equals the number of symbols that fit on the array along the worst possible direction, and using that many RF chains ensures one digital sample per symbol.

For planar arrays, the ratio between the RF chains required by digital and hybrid arrays is even more pronounced, as planar arrays can use space more efficiently [20].

Notably, the above points remain valid for suboptimum beamspace architectures, and in the case of linear arrays even for hybridly-connected structures, with the concomitant reduction in number of phase shifters; for hybridly-connected planar arrays, the reduction in phase shifters entails a tradeoff with the increase in RF chains. Readers are referred to Table III for a summary of the results.

Further research is required to determine whether similar behaviors are encountered with intelligent surfaces [45], in hybrid architectures with true-time-delay [15], [26], [46], [47], or in near-field situations [48]. Likewise, it could interesting to study whether the type of beamformer alters the interference on directions other than the one to the intended receiver.

Lastly, we hasten to emphasize that the scope of the paper has been LOS connectivity, where the only source of frequency selectivity is the beam squint itself. Then, the average beamforming gain, g_{avg} , maps one-to-one to performance measures such as the information-theoretic capacity or the error probability, and the condition $g_{avg} \approx N$ is necessary and sufficient for an N-antenna hybrid array to perform as a digital one. In channels with inherent frequency selectivity, say in multipath settings, this remains true when the number of antennas is large enough for the beamforming gain to harden around its mean value [49, Sec. 10.2]; for small antenna counts, conversely, g_{avg} no longer provides a complete description. In fact, in multipath settings it is usually possible to spatially multiplex various signal streams, and the beam squint phenomenon then generalizes to the so-called spatial wideband effect [14], [50]. Extending the analysis herein to that more general situation, with various concurrent beams, is yet another avenue for subsequent research.

ACKNOWLEDGMENT

The authors thank the Associate Editor and the anonymous reviewers for their valuable comments and suggestions.

APPENDIX A

As the smallest solution to (29) lies within the main lobe, it suffices to consider $0<\alpha_{\rm 3dB}<2$ and the problem reduces to

$$\frac{\sin\frac{\pi\alpha_{3dB}}{2}}{N\sin\frac{\pi\alpha_{3dB}}{2N}} = \frac{1}{\sqrt{2}}.$$
 (124)

Manipulating the left-hand side into

$$\frac{\sin\frac{\pi\alpha_{3dB}}{2}}{N\sin\frac{\pi\alpha_{3dB}}{2N}} = \frac{\sin\frac{\pi\alpha_{3dB}}{2}}{\frac{\pi\alpha_{3dB}}{2}} \cdot \frac{\frac{\pi\alpha_{3dB}}{2N}}{\sin\frac{\pi\alpha_{3dB}}{2N}}$$
(125)

shows that it is decreasing in N. Paired with the fact that the left-hand side is decreasing in α_{3dB} , the solution of (124) is decreasing with respect to N.

APPENDIX B

Combining $\lambda_{\ell}(\mathcal{B}_{\alpha}) \leq 1$ and $\sum_{\ell} \lambda_{\ell}(\mathcal{B}_{\alpha}) = \alpha$, we have that

$$\sum_{\ell < N_{\mathsf{RF}}} \lambda_n(\mathcal{B}_{\alpha}) \le \min(p, 1)\alpha. \tag{126}$$

In turn, for $\epsilon > 0$, we also have that

$$\sum_{\ell < N_{\mathsf{DF}}} \lambda_{\ell}(\mathcal{B}_{\alpha}) > \epsilon |\{\ell : \lambda_{\ell}(\mathcal{B}_{\alpha}) > \epsilon, \ell < N_{\mathsf{RF}}\}|$$
 (127)

$$= \epsilon \min(\alpha + \mathcal{O}(\log \alpha), \lceil p\alpha \rceil) \tag{128}$$

where the last equality follows from (51). Consequently

$$\liminf_{\alpha \to \infty} \frac{\sum_{\ell < N_{\mathsf{RF}}} \lambda_{\ell}(\mathcal{B}_{\alpha})}{\alpha}$$

$$\geq \epsilon \liminf_{\alpha \to \infty} \frac{\min(\alpha + \mathcal{O}(\log \alpha), \lceil p\alpha \rceil)}{\alpha} \tag{129}$$

where, as the existence of the limit is not guaranteed at this point, limit inferior was used.

For ϵ arbitrarily close to 1,

$$\liminf_{\alpha \to \infty} \frac{\sum_{\ell < N_{\mathsf{RF}}} \lambda_{\ell}(\mathcal{B}_{\alpha})}{\alpha} = \min(p, 1).$$
(131)

From (126), the limit inferior and limit superior coincide, hence the limit does exist and it equals min(p, 1) as desired.

APPENDIX C From $\int_{-\infty}^{\infty} \left(\frac{\sin \pi t}{\pi t}\right)^2 dt = 1$, which is straightforward from

$$\frac{1}{\alpha} \sum_{\ell < \lceil p\alpha \rceil} \int_{\ell - \frac{\lceil p\alpha \rceil - 1}{2} - \frac{\alpha}{2}}^{\ell - \frac{\lceil p\alpha \rceil - 1}{2} + \frac{\alpha}{2}} \left(\frac{\sin \pi t}{\pi t} \right)^2 dt \le \frac{\lceil p\alpha \rceil}{\alpha}. \tag{132}$$

Also, it can be shown that

$$\frac{1}{\alpha} \sum_{\ell < \lceil p\alpha \rceil} \int_{\ell - \frac{\lceil p\alpha \rceil - 1}{2} - \frac{\alpha}{2}}^{\ell - \frac{\lceil p\alpha \rceil - 1}{2} + \frac{\alpha}{2}} \left(\frac{\sin \pi t}{\pi t} \right)^{2} dt$$

$$\leq \frac{1}{\alpha} \int_{-\frac{\lceil p\alpha \rceil - 1}{2} - \frac{\alpha}{2}}^{-\frac{\lceil p\alpha \rceil - 1}{2} - \frac{\alpha}{2}} \underbrace{\sum_{\ell} \left(\frac{\sin \pi (t + \ell)}{\pi (t + \ell)} \right)^{2}}_{-1} dt = 1, \quad (133)$$

where the last identity follows from Poisson summation formula [51, Problem 6.2]. Combining them, we obtain

$$\limsup_{\alpha \to \infty} \frac{1}{\alpha} \sum_{\ell < \lceil p\alpha \rceil} \int_{\ell - \frac{\lceil p\alpha \rceil - 1}{2} - \frac{\alpha}{2}}^{\ell - \frac{\lceil p\alpha \rceil - 1}{2} + \frac{\alpha}{2}} \left(\frac{\sin \pi t}{\pi t} \right)^2 dt \le \min(p, 1).$$
(134)

At the same time, for $\epsilon > 0$ we can manipulate (59) as in (135)–(138), where (135) arises by imposing additional constraint on the summation index, (136) by restricting the interval of integration, (137) by factoring out the constant term with respect to the summation index, and (138) by computing the limit. Hence,

$$\liminf_{\alpha \to \infty} \frac{1}{\alpha} \sum_{\ell < \lceil p\alpha \rceil} \int_{\ell - \frac{\lceil p\alpha \rceil - 1}{2} - \frac{\alpha}{2}}^{\ell - \frac{\lceil p\alpha \rceil - 1}{2} + \frac{\alpha}{2}} \left(\frac{\sin \pi t}{\pi t} \right)^{2} dt$$

$$\geq \min\left(p, \frac{1 + p - \epsilon}{2}\right) - \max\left(0, \frac{-1 + p + \epsilon}{2}\right). \quad (139)$$

For an arbitrarily small $\epsilon > 0$,

$$\liminf_{\alpha \to \infty} \frac{1}{\alpha} \sum_{\ell < \lceil p\alpha \rceil} \int_{\ell - \frac{\lceil p\alpha \rceil - 1}{2} - \frac{\alpha}{2}}^{\ell - \frac{\lceil p\alpha \rceil - 1}{2} + \frac{\alpha}{2}} \left(\frac{\sin \pi t}{\pi t}\right)^2 dt$$

$$\geq \min\left(p, \frac{1+p}{2}\right) - \max\left(0, \frac{-1+p}{2}\right) = \min(p, 1), (140)$$

which concludes the proof.

APPENDIX D

This appendix identifies the maximum and minimum of

$$\frac{1}{W} \int_{-\frac{W}{2}}^{\frac{W}{2}} \frac{g_{\rm t}(f)g_{\rm r}(f)}{N_{\rm t}N_{\rm r}} df \tag{141}$$

under the constraints

$$0 \le g_{\rm t}(f) \le N_{\rm t} \qquad \frac{1}{W} \int_{-\frac{W}{2}}^{\frac{W}{2}} g_{\rm t}(f) df = g_{\rm avg,t}$$

$$0 \le g_{\rm r}(f) \le N_{\rm r} \qquad \frac{1}{W} \int_{-\frac{W}{2}}^{\frac{W}{2}} g_{\rm r}(f) df = g_{\rm avg,r}. \tag{142}$$

Introducing

(130)

$$f_{\rm t}(t) \equiv \frac{g_{\rm t}\left(W\left(t-\frac{1}{2}\right)\right)}{N_{\rm t}} \qquad f_{\rm r}(t) \equiv \frac{g_{\rm r}\left(W\left(t-\frac{1}{2}\right)\right)}{N_{\rm r}}, \quad (143)$$

the objective and the constraints become

$$\int_0^1 f_{\mathbf{t}}(t) f_{\mathbf{r}}(t) df \tag{144}$$

and

$$0 \le f_{\mathbf{t}}(t) \le 1 \qquad \int_{0}^{1} f_{\mathbf{t}}(t) df = g_{\mathsf{avg},\mathbf{t}}$$

$$0 \le f_{\mathbf{r}}(t) \le 1 \qquad \int_{0}^{1} f_{\mathbf{r}}(t) df = g_{\mathsf{avg},\mathbf{r}}. \tag{145}$$

Commencing with the maximum value,

$$\int_{0}^{1} f_{t}(t) f_{r}(t) dt \le \int_{0}^{1} f_{t}(t) dt = g_{\text{avg},t}.$$
 (146)

Repeating the argument gives

$$\int_{0}^{1} f_{t}(t) f_{r}(t) dt \le \int_{0}^{1} f_{r}(t) dt = g_{\text{avg,r}}.$$
 (147)

Combining the bounds,

$$\int_{0}^{1} f_{t}(t) f_{r}(t) dt \le \min \left(g_{\text{avg,t}}, g_{\text{avg,r}} \right)$$
 (148)

This bound is tight in that it can be attained by

$$f_{\rm t}(t) = [0 \le t \le g_{\rm avg,t}]$$
 $f_{\rm r}(t) = [0 \le t \le g_{\rm avg,r}].$ (149)

Turning to the minimum value, it can be obtained from the observation that

$$\int_{0}^{1} (1 - f_{t}(t))(1 - f_{r}(t))dt \ge 0, \tag{150}$$

which is equivalent to

$$\int_{0}^{1} f_{t}(t) f_{r}(t) dt \ge g_{\text{avg},t} + g_{\text{avg},r} - 1.$$
 (151)

$$\frac{1}{\alpha} \sum_{\ell < \lceil p\alpha \rceil} \int_{\ell - \frac{\lceil p\alpha \rceil - 1}{2} - \frac{\alpha}{2}}^{\ell - \frac{\lceil p\alpha \rceil - 1}{2} + \frac{\alpha}{2}} \left(\frac{\sin \pi t}{\pi t} \right)^2 dt$$

$$\geq \frac{1}{\alpha} \sum_{\ell} \left[0 \leq \ell < \lceil p\alpha \rceil \right] \left[\ell - \frac{\lceil p\alpha \rceil - 1}{2} + \frac{\alpha}{2} > \epsilon \alpha \right] \left[\ell - \frac{\lceil p\alpha \rceil - 1}{2} - \frac{\alpha}{2} < -\epsilon \alpha \right] \int_{\ell - \frac{\lceil p\alpha \rceil - 1}{2} - \frac{\alpha}{2}}^{\ell - \frac{\lceil p\alpha \rceil - 1}{2} + \frac{\alpha}{2}} \left(\frac{\sin \pi t}{\pi t} \right)^2 dt \tag{135}$$

$$\geq \frac{1}{\alpha} \sum_{\ell} \left[0 \leq \ell < \lceil p\alpha \rceil \right] \left[\ell - \frac{\lceil p\alpha \rceil - 1}{2} + \frac{\alpha}{2} > \epsilon \alpha \right] \left[\ell - \frac{\lceil p\alpha \rceil - 1}{2} - \frac{\alpha}{2} < -\epsilon \alpha \right] \int_{-\epsilon \alpha}^{\epsilon \alpha} \left(\frac{\sin \pi t}{\pi t} \right)^2 dt \tag{136}$$

$$= \left(\frac{1}{\alpha} \sum_{\ell} \left[0 \le \ell < \lceil p\alpha \rceil\right] \left[\ell - \frac{\lceil p\alpha \rceil - 1}{2} + \frac{\alpha}{2} > \epsilon \alpha\right] \left[\ell - \frac{\lceil p\alpha \rceil - 1}{2} - \frac{\alpha}{2} < -\epsilon \alpha\right]\right) \int_{-\epsilon \alpha}^{\epsilon \alpha} \left(\frac{\sin \pi t}{\pi t}\right)^2 dt \tag{137}$$

$$\to \min\left(p, \frac{1+p-\epsilon}{2}\right) - \max\left(0, \frac{-1+p+\epsilon}{2}\right) \tag{138}$$

Together with the nonnegativity, we have that

$$\int_{0}^{1} f_{t}(t) f_{r}(t) dt \ge \max \left(g_{\text{avg},t} + g_{\text{avg},r} - 1, 0 \right).$$
 (152)

This bound can be attained by

$$f_{\rm t}(t) = [0 \le t \le g_{\rm avg,t}]$$
 $f_{\rm r}(t) = [1 - g_{\rm avg,r} \le t \le 1].$ (153)

APPENDIX E

Let us consider a spectral decomposition of \tilde{B}_{α} ,

$$\tilde{B}_{\alpha}(\tilde{r}'_x, \tilde{r}_x) = \sum_{\ell} \lambda_{\ell} u_{\ell}(\tilde{r}'_x) \overline{u_{\ell}(r_x)}, \tag{154}$$

where $\{u_\ell\}$ is a set of orthonormal functions. Multiplying both sides with

$$\frac{\left[\tilde{r} \in RA\right]}{\left(\int \left[\tilde{r} \in RA\right] d\tilde{r}_{y}\right)^{\frac{1}{2}}} \cdot \frac{\left[\tilde{r}' \in RA\right]}{\left(\int \left[\tilde{r}' \in RA\right] d\tilde{r}'_{y}\right)^{\frac{1}{2}}},$$
 (155)

the left- and right-hand sides of (154) become respectively (79) and

$$\sum_{\ell} \lambda_{\ell} \tilde{u}_{\ell}(\tilde{r}') \overline{\tilde{u}_{\ell}(\tilde{r})}, \tag{156}$$

where

$$\tilde{u}_{\ell}(\tilde{r}) = \frac{\left[\tilde{r} \in RA\right]}{\left(\int \left[\tilde{r} \in RA\right] d\tilde{r}_{y}\right)^{\frac{1}{2}}} u_{\ell}(\tilde{r}_{x}). \tag{157}$$

We can easily verify the orthonormality of (157) from

$$\iint \frac{\left[\tilde{r} \in \mathbf{R}A\right]}{\int \left[\tilde{r} \in \mathbf{R}A\right] d\tilde{r}_{y}} u_{\ell}(\tilde{r}_{x}) \overline{u_{\ell'}(\tilde{r}_{x})} d\tilde{r}_{x} d\tilde{r}_{y}$$
(158)

$$= \int \left(\int \frac{\left[\tilde{\boldsymbol{r}} \in \boldsymbol{R} A \right]}{\int \left[\tilde{\boldsymbol{r}} \in \boldsymbol{R} A \right] d\tilde{r}_{y}} d\tilde{r}_{y} \right) u_{\ell}(\tilde{r}_{x}) \overline{u_{\ell'}(\tilde{r}_{x})} d\tilde{r}_{x} \quad (159)$$

$$= \int u_{\ell}(\tilde{r}_x) \overline{u_{\ell'}(\tilde{r}_x)} d\tilde{r}_x, \tag{160}$$

implying that (156) is a spectral decomposition of \mathcal{B}_{α} . Thus, $\{\lambda_{\ell}\}$, the eigenvalues of $\tilde{\mathcal{B}}_{\alpha}$, are also the eigenvalues of \mathcal{B}_{α} .

APPENDIX F

Let $\mathcal L$ be a positive semi-definite Hilbert-Schmidt operator with kernel L(t,t') and let $\mathcal G$ be an operator satisfying $(\mathcal Gs)(t)=g(t)s(t)$ with $g\in L^2(\mathbb R)$ and $0\leq |g(t)|\leq 1$ for all t. We wish to prove that

$$\lambda_{\ell}(\mathcal{GLG}) \le \lambda_n(\mathcal{L}),$$
 (161)

which is a broader result subsuming (87). The min-max theorem for matrices [33, Thm. 4.2.6], which can be naturally generalized to self-adjoint Hilbert-Schmidt operators, does the trick. Applying it, it can be seen that

$$\lambda_{\ell}(\mathcal{GLG}) = \min_{\varphi \in \mathsf{span}(\psi_0, \dots, \psi_{\ell}), \varphi \neq 0} \frac{\langle \mathcal{GLG}\varphi, \varphi \rangle}{\langle \varphi, \varphi \rangle}$$
(162)

$$= \min_{\varphi \in \mathsf{span}(\psi_0, \dots, \psi_\ell), \varphi \neq 0} \frac{\langle \mathcal{LG}\varphi, \mathcal{G}\varphi \rangle}{\langle \varphi, \varphi \rangle} \tag{163}$$

$$\leq \min_{\tilde{\varphi} \in \operatorname{span}(\mathcal{G}\psi_0, \dots, \mathcal{G}\psi_\ell), \tilde{\varphi} \neq 0} \frac{\langle \mathcal{L}\tilde{\varphi}, \tilde{\varphi} \rangle}{\langle \tilde{\varphi}, \tilde{\varphi} \rangle} \tag{164}$$

$$\leq \max_{\dim(S)=\ell+1} \min_{\tilde{\varphi}\in S, \tilde{\varphi}\neq 0} \frac{\langle \mathcal{L}\tilde{\varphi}, \tilde{\varphi}\rangle}{\langle \tilde{\varphi}, \tilde{\varphi}\rangle}$$
(165)

$$=\lambda_{\ell}(\mathcal{L}),\tag{166}$$

where ψ_k is the eigenvector of \mathcal{GLG} corresponding to the kth largest eigenvalue. The first inequality follows from the substitution $\tilde{\varphi} = \mathcal{G}\varphi$ and $\|\tilde{\varphi}\| \leq \|\varphi\|$.

APPENDIX G

This appendix proves that (92) holds if and only if $p \ge 1$.

A. Sufficiency

The sufficiency requires (92) to vanish if $p \ge 1$. Using (53) and (87)

$$\sum_{\ell > \lceil p\alpha^{\mathsf{up}} \rceil} \lambda_{\ell}(\mathcal{B}_{\alpha}) \le L_3 \sum_{\ell > \lceil p\alpha^{\mathsf{up}} \rceil} \lambda_{\ell}(\mathcal{B}_{\alpha^{\mathsf{up}}}) \tag{167}$$

$$= L_3 \alpha^{\mathsf{up}} \max(0, 1 - p) + o(r). \tag{168}$$

Therefore,

$$\frac{\sum_{\ell \ge \lceil p\alpha^{\mathsf{up}} \rceil} \lambda_{\ell}(\mathcal{B}_{\alpha})}{\sum_{\ell} \lambda_{\ell}(\mathcal{B}_{\alpha})} \le \frac{L_{3}\alpha^{\mathsf{up}} \max(0, 1 - p) + o(r)}{\|\alpha\|} \quad (169)$$

which does converge to zero if $p \geq 1$. Recall that $\frac{\alpha^{\text{up}}}{\|\alpha\|}$ is constant with respect to r.

B. Necessity

The necessity requires (92) not to vanish for p < 1. From (53) and (87),

$$\frac{\sum_{\ell \ge \lceil p\alpha^{\mathsf{up}} \rceil} \lambda_{\ell}(\mathcal{B}_{\alpha})}{\sum_{\ell} \lambda_{\ell}(\mathcal{B}_{\alpha})} \ge \frac{\delta L_{3} \alpha^{\mathsf{lo}} \max(0, 1 - \frac{\alpha^{\mathsf{up}}}{\alpha^{\mathsf{lo}}} p) + o(r)}{\|\alpha\|}.$$
(170)

Recall that both $\frac{\alpha^{\text{lo}}}{\|\alpha\|}$ and $\frac{\alpha^{\text{up}}}{\alpha^{\text{lo}}}$ are constant with respect to r. From p<1, a small enough $\delta>0$ can be chosen such that

$$\frac{\alpha^{\sf up}}{\alpha^{\sf lo}}p = \frac{L_1}{(1-\delta)L_1 + \delta L_2}p < 1.$$
 (171)

Therefore, (170) cannot vanish.

APPENDIX H

One welcome property of a partially-connected architecture is that, if the subarrays are identical, both in topology and in the number of phase shifts, one can replace their individual RF chains with delay lines and connect all of them to a single RF chain without loss in performance. While the result for linear arrays with MRT beamformer can be found in [10, Sec. I-B] (also in [25, Prop. 1] and [26, Sec. III-D]), this appendix extends the result for completeness.

Precisely, the first condition corresponds to

$$\boldsymbol{a}_{m}^{*}(f) = \exp\left(j2\pi \frac{f_{c} + f}{c} \boldsymbol{u}^{\top} \overline{\boldsymbol{r}}_{m}\right) \boldsymbol{a}_{0}^{*}(f)$$
 (172)

where \overline{r}_m is the displacement of the mth subarray with respect to the 0th one (recall (4)). The second condition is

$$\mathbf{W}_{\mathsf{a}} = \mathsf{blkdiag}(\mathbf{w}_{\mathsf{a}}, \dots, \mathbf{w}_{\mathsf{a}}) \tag{173}$$

where $w_{\mathsf{a}} \in \mathbb{C}^{\frac{N}{M}}$ is the subarray beamformer.

From the block diagonal structure (173), the beamforming gain in (12) is reduced to

$$g(f) = \frac{\left| \left(\sum_{m} \boldsymbol{a}_{m}^{*}(f) [\boldsymbol{w}_{\mathsf{d}}(f)]_{m} \right) \boldsymbol{w}_{\mathsf{a}} \right|^{2}}{\|\boldsymbol{w}_{\mathsf{a}}\|^{2} \|\boldsymbol{w}_{\mathsf{d}}(f)\|^{2}}, \tag{174}$$

Armed with (172), it can be recast as

$$\frac{\left|\sum_{m} \exp\left(j2\pi \frac{f_{c}+f}{c} \boldsymbol{u}^{\top} \overline{\boldsymbol{r}}_{m}\right) [\boldsymbol{w}_{d}(f)]_{m}\right|^{2}}{\|\boldsymbol{w}_{d}(f)\|^{2}} \cdot \frac{|\boldsymbol{a}_{0}^{*}(f) \boldsymbol{w}_{a}|^{2}}{\|\boldsymbol{w}_{a}\|^{2}}.$$
(175)

Applying the Cauchy-Schwarz inequality,

$$g(f) \le Mg_0(f), \tag{176}$$

and the equality is seen to be attained by

$$[\boldsymbol{w}_{\mathsf{d}}(f)]_{m} = \exp\left(-j2\pi \frac{f_{\mathsf{c}} + f}{c} \boldsymbol{u}^{\mathsf{T}} \overline{\boldsymbol{r}}_{m}\right),$$
 (177)

which can be implemented with delay lines. This maximum beamforming gain equals (101), obtained with M RF chains.

The resulting architecture with delay lines mitigates the beam squint across the subarrays. The remainder, the beam squint within the subarray, is relatively negligible. This very idea has recently applied to a multipath setting in [25], [26].

REFERENCES

- H. Do, S. Cho, J. Park, H.-J. Song, N. Lee, and A. Lozano, "Terahertz line-of-sight MIMO communication: Theory and practical challenges," *IEEE Commun. Mag.*, vol. 59, no. 3, pp. 104–109, 2021.
- [2] F. Boccardi, R. W. Heath, A. Lozano, T. L. Marzetta, and P. Popovski, "Five disruptive technology directions for 5G," *IEEE Commun. Mag.*, vol. 52, no. 2, pp. 74–80, 2014.
- [3] J. G. Andrews, S. Buzzi, W. Choi, S. V. Hanly, A. Lozano, A. C. Soong, and J. C. Zhang, "What will 5G be?" *IEEE J. Sel. Areas Commun.*, vol. 32, no. 6, pp. 1065–1082, 2014.
- [4] S. Rangan, T. S. Rappaport, and E. Erkip, "Millimeter-wave cellular wireless networks: Potentials and challenges," *Proc. IEEE*, vol. 102, no. 3, pp. 366–385, 2014.
- [5] A. L. Swindlehurst, E. Ayanoglu, P. Heydari, and F. Capolino, "Millimeter-wave massive MIMO: The next wireless revolution?" *IEEE Commun. Mag.*, vol. 52, no. 9, pp. 56–62, 2014.
- [6] X. Zhang, A. F. Molisch, and S.-Y. Kung, "Variable-phase-shift-based RF-baseband codesign for MIMO antenna selection," *IEEE Trans. Signal Process.*, vol. 53, no. 11, pp. 4091–4103, 2005.
- [7] F. Sohrabi and W. Yu, "Hybrid digital and analog beamforming design for large-scale antenna arrays," *IEEE J. Sel. Topics Signal Process.*, vol. 10, no. 3, pp. 501–513, 2016.
- [8] O. El Ayach, S. Rajagopal, S. Abu-Surra, Z. Pi, and R. W. Heath, "Spatially sparse precoding in millimeter wave MIMO systems," *IEEE Trans. Wireless Commun.*, vol. 13, no. 3, pp. 1499–1513, 2014.
- [9] R. J. Mailloux, *Phased array antenna handbook*, 2nd ed. Artech house, 2005
- [10] —, "Phased array theory and technology," Proc. IEEE, vol. 70, no. 3, pp. 246–291, 1982.
- [11] R. Rotman, M. Tur, and L. Yaron, "True time delay in phased arrays," *Proc. IEEE*, vol. 104, no. 3, pp. 504–518, 2016.
- [12] M. Longbrake, "True time-delay beamsteering for radar," in *IEEE Nat. Aerosp. Electron. Conf.*, 2012, pp. 246–249.
- [13] Z. Cao, Q. Ma, A. B. Smolders, Y. Jiao, M. J. Wale, C. W. Oh, H. Wu, and A. M. J. Koonen, "Advanced integration techniques on broadband millimeter-wave beam steering for 5G wireless networks and beyond," *IEEE J. Quantum Electron.*, vol. 52, no. 1, pp. 1–20, 2015.
- [14] M. M. Mojahedian, M. Attarifar, and A. Lozano, "Spatial-wideband effect in line-of-sight MIMO communication," in *IEEE Int'l Conf.* Commun., 2022, pp. 3972–3977.
- [15] L. Steinweg, C. Carta, and F. Ellinger, "A hybrid true-time and phase-delayed approach for millimeter-wave beam steering," *IEEE Trans. Microwave Theory Techn.*, vol. 70, no. 9, pp. 4318–4327, 2022.
- [16] C.-C. Lin et al., "Wideband beamforming with rainbow beam training using reconfigurable true-time-delay arrays for millimeter-wave wireless," *IEEE Circuits Syst. Mag.*, vol. 22, no. 4, pp. 6–25, 2022.
- [17] X. Liu and D. Qiao, "Space-time block coding-based beamforming for beam squint compensation," *IEEE Wireless Commun. Lett.*, vol. 8, no. 1, pp. 241–244, 2018.
- [18] F. Gao, B. Wang, C. Xing, J. An, and G. Y. Li, "Wideband beamforming for hybrid massive MIMO terahertz communications," *IEEE J. Sel. Areas Commun.*, vol. 39, no. 6, pp. 1725–1740, 2021.
- [19] M. Ma, N. T. Nguyen, and M. Juntti, "Closed-form hybrid beamforming solution for spectral efficiency upper bound maximization in mmWave MIMO-OFDM systems," in *IEEE Veh. Technol. Conf.*, 2021, pp. 1–5.
- [20] N. T. Nguyen, J. Kokkoniemi, and M. Juntti, "Beam squint effects in THz communications with UPA and ULA: Comparison and hybrid beamforming design," in *IEEE Global Commun. Conf. Workshops*, 2022, pp. 1754–1759.
- [21] A. M. Elbir, "A unified approach for beam-split mitigation in terahertz wideband hybrid beamforming," *IEEE Trans. Veh. Technol.*, vol. 72, no. 9, pp. 12355–12360, 2023.
- [22] M. Cai, K. Gao, D. Nie, B. Hochwald, J. N. Laneman, H. Huang, and K. Liu, "Effect of wideband beam squint on codebook design in phased-array wireless systems," in *IEEE Global Commun. Conf.*, 2016, pp. 1–6.
- [23] M. Cai, J. N. Laneman, and B. Hochwald, "Beamforming codebook compensation for beam squint with channel capacity constraint," in *IEEE Int'l Symp. Inf. Theory*, 2017, pp. 76–80.
- [24] B. Wang, M. Jian, F. Gao, G. Y. Li, and H. Lin, "Beam squint and channel estimation for wideband mmwave massive MIMO-OFDM systems," *IEEE Trans. Signal Process.*, vol. 67, no. 23, pp. 5893–5908, 2019.
- [25] K. Dovelos, M. Matthaiou, H. Q. Ngo, and B. Bellalta, "Channel estimation and hybrid combining for wideband terahertz massive MIMO

- systems," *IEEE J. Sel. Areas Commun.*, vol. 39, no. 6, pp. 1604–1620, 2021.
- [26] L. Dai, J. Tan, Z. Chen, and H. V. Poor, "Delay-phase precoding for wideband THz massive MIMO," *IEEE Trans. Wireless Commun.*, vol. 21, no. 9, pp. 7271–7286, 2022.
- [27] J. H. Brady and A. M. Sayeed, "Wideband communication with high-dimensional arrays: New results and transceiver architectures," in *IEEE Int'l Conf. Commun. Workshop*, 2015, pp. 1042–1047.
- [28] W. H. Von Aulock, "Properties of phased arrays," Proc. IRE, vol. 48, no. 10, pp. 1715–1727, 1960.
- [29] H.-J. Song and T. Nagatsuma, "Present and future of terahertz communications," *IEEE Trans. Terahertz Sci. Technol.*, vol. 1, no. 1, pp. 256–263, 2011.
- [30] A. Alkhateeb and R. W. Heath, "Frequency selective hybrid precoding for limited feedback millimeter wave systems," *IEEE Trans. Commun.*, vol. 64, no. 5, pp. 1801–1818, 2016.
- [31] R. C. Hansen, Phased array antennas, 2nd ed. John Wiley & Sons, 2009.
- [32] S. Park, A. Alkhateeb, and R. W. Heath, "Dynamic subarrays for hybrid precoding in wideband mmWave MIMO systems," *IEEE Trans. Wireless Commun.*, vol. 16, no. 5, pp. 2907–2920, 2017.
- [33] R. A. Horn and C. R. Johnson, *Matrix analysis*, 2nd ed. Cambridge university press, 2013.
- [34] H. Do, N. Lee, and A. Lozano, "Line-of-sight MIMO via intelligent reflecting surface," *IEEE Trans. Wireless Commun.*, vol. 22, no. 6, pp. 4215–4231, 2023.
- [35] D. E. Knuth, "Two notes on notation," The American Mathematical Monthly, vol. 99, no. 5, pp. 403–422, 1992.
- [36] H. J. Landau and H. Widom, "Eigenvalue distribution of time and frequency limiting," *J. Math. Anal. Appl.*, vol. 77, no. 2, pp. 469–481, 1980.
- [37] D. Slepian and H. O. Pollak, "Prolate spheroidal wave functions, Fourier analysis and uncertainty—I," *Bell System Tech. J.*, vol. 40, no. 1, pp. 43–63, 1961.
- [38] M. Dohler, R. W. Heath, A. Lozano, C. B. Papadias, and R. A. Valenzuela, "Is the PHY layer dead?" *IEEE Commun. Mag.*, vol. 49, no. 4, pp. 159–165, 2011.
- [39] A. Townsend and L. N. Trefethen, "An extension of chebfun to two dimensions," SIAM J. Scientific Comput., vol. 35, no. 6, pp. C495– C518, 2013.
- [40] D. Zhang, Y. Wang, X. Li, and W. Xiang, "Hybridly connected structure for hybrid beamforming in mmwave massive MIMO systems," *IEEE Trans. Commun.*, vol. 66, no. 2, pp. 662–674, 2017.
- [41] C. Singhal and S. De, Resource allocation in next-generation broadband wireless access networks. IGI Global, 2017.
- [42] A. Lozano and S. Rangan, "Spectral vs energy efficiency in 6G: Impact of the receiver front-end," *IEEE BITS Inf. Theory Mag.*, 2023.
- [43] S. Wesemann, J. Du, and H. Viswanathan, "Energy efficient extreme MIMO: Design goals and directions," *IEEE Commun. Mag.*, vol. 61, no. 10, pp. 132–138, 2023.
- [44] H. Do, N. Lee, and A. Lozano, "Parabolic wavefront model for line-ofsight MIMO channels," *IEEE Trans. Wireless Commun.*, vol. 22, no. 11, pp. 7620–7634, 2023.
- [45] S.-H. Park, B. Kim, D. K. Kim, L. Dai, K.-K. Wong, and C.-B. Chae, "Beam squint in ultra-wideband mmWave systems: RF lens array vs. phase-shifter-based array," *IEEE Wireless Commun.*, vol. 30, no. 4, pp. 82–89, 2023.
- [46] B. Zhai, Y. Zhu, A. Tang, and X. Wang, "THzPrism: Frequency-based beam spreading for terahertz communication systems," *IEEE Wireless Commun. Lett.*, vol. 9, no. 6, pp. 897–900, 2020.
- [47] I. K. Jain, R. R. Vennam, R. Subbaraman, and D. Bharadia, "mmFlexible: Flexible directional frequency multiplexing for multi-user mmwave networks," in *IEEE Int'l Conf. Comput. Commun.*, 2023.
- [48] N. J. Myers and R. W. Heath, "InFocus: A spatial coding technique to mitigate misfocus in near-field LoS beamforming," *IEEE Trans. Wireless Commun.*, vol. 21, no. 4, pp. 2193–2209, 2021.
- [49] R. W. Heath, Jr. and A. Lozano, Foundations of MIMO Communication. Cambridge University Press, 2018.
- [50] B. Wang, F. Gao, S. Jin, H. Lin, G. Y. Li, S. Sun, and T. S. Rappaport, "Spatial-wideband effect in massive MIMO with application in mmWave systems," *IEEE Commun. Mag.*, vol. 56, no. 12, pp. 134– 141, 2018.
- [51] B. G. Osgood, Lectures on the Fourier transform and its applications. Amer. Math. Soc., 2019, vol. 33.



Heedong Do (S'20 – M'23) received a B.S. in mathematics and a Ph.D. in electrical engineering from Pohang University of Science & Technology (POSTECH), Pohang, Korea, in 2018 and 2023, respectively. He is currently a postdoctoral associate at Korea University.



Namyoon Lee (S'11–M'14–SM'20) received a Ph.D. degree from The University of Texas at Austin, in 2014. He was with Communications and Network Research Group, Samsung Advanced Institute of Technology (SAIT), Korea, in 2008-2011 and also with Wireless Communications Research (WCR), Intel Labs, Santa Clara, USA, in 2015-2016. He was with POSTECH, Pohang, Gyeongbuk in 2016-2022, Korea and is currently an Associate Professor at Korea University, Seoul, Korea. He was a recipient of the 2016 IEEE ComSoc Asia–Pacific

Outstanding Young Researcher Award. He is currently an Editor for the IEEE Trans. on Wireless Communications and IEEE Trans. on Communications.



Robert W. Heath Jr. (S'96 - M'01 - SM'06 - F'11) is the Charles Lee Powell Chair in Wireless Communications in the Department of Electrical and Computer Engineering at the University of California, San Diego. He is also President and CEO of MIMO Wireless Inc. From 2002-2020 he was with The University of Texas at Austin, most recently as Cockrell Family Regents Chair in Engineering and Director of UT SAVES. From 2020-2023 he was the Lampe Distinguished Professor at North Carolina State University and co-founder of 6GNC. He He

authored "Introduction to Wireless Digital Communication" (Prentice Hall, 2017) and "Digital Wireless Communication: Physical Layer Exploration Lab Using the NI USRP" (National Technology and Science Press, 2012), and coauthored "Millimeter Wave Wireless Communications" (Prentice Hall, 2014) and "Foundations of MIMO Communication" (Cambridge University Press, 2018)

Dr. Heath has been a co-author of a number award winning conference and journal papers including recently the 2017 Marconi Prize Paper Award, the 2019 IEEE Communications Society Stephen O. Rice Prize, the 2020 IEEE Signal Processing Society Donald G. Fink Overview Paper Award, the 2021 IEEE Vehicular Technology Society Neal Shepherd Memorial Best Propagation Paper Award, and the 2022 IEEE Vehicular Technology Society Best Vehicular Electronics Paper Award. Other notable awards include the 2017 EURASIP Technical Achievement award, the 2019 IEEE Kiyo Tomiyasu Award and the 2021 IEEE Vehicular Technology Society James Evans Avant Garde Award. In 2017, he was selected as a Fellow of the National Academy of Inventors. He was a member-at-large on the IEEE Communications Society Board-of-Governors (2020-2022) and the IEEE Signal Processing Society Board-of-Governors (2016-2018). He was Editor-in-Chief of IEEE Signal Processing Magazine from 2018-2020. He is also a licensed Amateur Radio Operator, a Private Pilot, a registered Professional Engineer in Texas.



Angel Lozano (S'90 – M'99– SM'01 - F'14) received a Ph.D. from Stanford University in 1998. From 1999 to 2008 he was with Bell Labs (Lucent Technologies, now Nokia). He is currently a Professor at Univ. Pompeu Fabra (UPF), Barcelona, and the co-author of the textbook "Foundations of MIMO Communication" (Cambridge University Press, 2019). He serves as Area Editor for the IEEE Trans. on Wireless Communications. He received the 2009 Stephen O. Rice Prize, the 2016 Fred W. Ellersick prize, and the 2016 Communications

Society & Information Theory Society joint paper award. He holds an Advanced Grant from the European Research Council and was a 2017 Clarivate Analytics Highly Cited Researcher.